Journal of Orthopaedic Translation 47 (2024) 161–175

Contents lists available at ScienceDirect

Journal of Orthopaedic Translation

journal homepage: www.journals.elsevier.com/journal-of-orthopaedic-translation

Original Article

Roles of Sp7 in osteoblasts for the proliferation, differentiation, and osteocyte process formation

Qing Jiang [a,b], Kenichi Nagano [c], Takeshi Moriishi [d], Hisato Komori [b], Chiharu Sakane [e], Yuki Matsuo [b,d], Zhiguo Zhang [f], Riko Nishimura [g], Kosei Ito [b], Xin Qin [a,b,**], Toshihisa Komori [b,*,1]

[a] Institute of Orthopaedics, Suzhou Medical College, Soochow University, Suzhou 215006, China
[b] Department of Molecular Bone Biology, Nagasaki University Graduate School of Biomedical Sciences, Nagasaki 852–8588, Japan
[c] Department of Oral Pathology and Bone Metabolism, Nagasaki University Graduate School of Biomedical Sciences, Nagasaki 852–8588, Japan
[d] Department of Cell Biology, Nagasaki University Graduate School of Biomedical Sciences, Nagasaki 852–8588, Japan
[e] Research Center for Biomedical Models and Animal Welfare, Nagasaki University Graduate School of Biomedical Sciences, Nagasaki, 852–8588, Japan
[f] Institute of Basic Theory for Chinese Medicine, China Academy of Chinese Medical Sciences, Beijing, 100700, China
[g] Department of Molecular and Cellular Biochemistry, Osaka University Graduate School of Dentistry, 1–8 Yamadaoka, Suita, Osaka 565–0871, Japan

ARTICLE INFO

Keywords:
Sp7
Osteoblast differentiation
Osteoblast proliferation
Osteocyte apoptosis
Osteocyte processes
Cortical porosity

ABSTRACT

Background: Zinc finger-containing transcription factor Osterix/Specificity protein-7 (Sp7) is an essential transcription factor for osteoblast differentiation. However, its functions in differentiated osteoblasts remain unclear and the effects of osteoblast-specific *Sp7* deletion on osteocytes have not been sufficiently studied.

Methods: $Sp7^{floxneo/floxneo}$ mice, in which *Sp7* expression was 30 % of that in wild-type mice because of disturbed splicing by neo gene insertion, and osteoblast-specific knockout ($Sp7^{fl/fl;Col1a1-Cre}$) mice using 2.3-kb *Col1a1* enhanced green fluorescent protein (EGFP)-Cre were examined by micro-computed tomography (micro-CT), bone histomorphometry, serum markers, and histological analyses. The expression of osteoblast and osteocyte marker genes was examined by real-time reverse transcription (RT)-PCR analysis. Osteoblastogenesis, osteoclastogenesis, and regulation of the expression of collagen type I alpha 1 chain (*Col1a1*) were examined in primary osteoblasts.

Results: Femoral trabecular bone volume was higher in female $Sp7^{floxneo/floxneo}$ and $Sp7^{fl/fl;Col1a1-Cre}$ mice than in the respective controls, but not in males. Bromodeoxyuridine (BrdU)-positive osteoblastic cells were increased in male $Sp7^{fl/fl;Col1a1-Cre}$ mice, and osteoblast number and the bone formation rate were increased in tibial trabecular bone in female $Sp7^{fl/fl;Col1a1-Cre}$ mice, although osteoblast maturation was inhibited in female $Sp7^{fl/fl;Col1a1-Cre}$ mice as shown by the increased expression of an immature osteoblast marker gene, secreted phosphoprotein 1 (*Spp1*), and reduced expression of a mature osteoblast marker gene, bone gamma-carboxyglutamate protein/bone gamma-carboxyglutamate protein 2 (*Bglap/Bglap2*). Furthermore, alkaline phosphatase activity was increased but mineralization was reduced in the culture of primary osteoblasts from $Sp7^{fl/fl;Col1a1-Cre}$ mice. Therefore, the accumulated immature osteoblasts in $Sp7^{fl/fl;Col1a1-Cre}$ mice was likely compensated for the inhibition of osteoblast maturation at different levels in males and females. Vertebral trabecular bone volume was lower in both male and female $Sp7^{fl/fl;Col1a1-Cre}$ mice than in the controls and the osteoblast parameters and bone formation rate in females were lower in $Sp7^{fl/fl;Col1a1-Cre}$ mice than in $Sp7^{fl/fl}$ mice, suggesting differential regulatory mechanisms in long bones and vertebrae. The femoral cortical bone was thin and porous in $Sp7^{floxneo/floxneo}$ and $Sp7^{fl/fl;Col1a1-Cre}$ mice of both sexes, the number of canaliculi was reduced, and terminal deoxynucleotidyl transferase-mediated dUTP nick end labelling (TUNEL)-positive lacunae and the osteoclasts were increased, whereas the bone formation rate was similar in $Sp7^{fl/fl;Col1a1-Cre}$ and $Sp7^{fl/fl}$ mice. The serum levels of total procollagen type 1 N-terminal propeptide (P1NP), a marker for bone formation, were similar, while those of tartrate-resistant acid phosphatase 5b (TRAP5b), a marker for bone resorption, were higher in $Sp7^{fl/fl;Col1a1-Cre}$

* Corresponding author.
** Corresponding author. Institute of Orthopaedics, Suzhou Medical College, Soochow University, Suzhou 215006, China.
E-mail addresses: xqin@suda.edu.cn (X. Qin), komorit@nagasaki-u.ac.jp (T. Komori).
[1] Lead contact

https://doi.org/10.1016/j.jot.2024.06.005
Received 4 March 2024; Received in revised form 22 May 2024; Accepted 2 June 2024

mice. Osteoblasts were less cuboidal, the expression of *Col1a1* and *Col1a1*-EGFP-Cre was lower in $Sp7^{fl/fl;Col1a1-Cre}$ mice, and overexpression of *Sp7* induced *Col1a1* expression.

Conclusions: Our studies indicated that Sp7 inhibits the proliferation of immature osteoblasts, induces osteoblast maturation and *Col1a1* expression, and is required for osteocytes to acquire a sufficient number of processes for their survival, which prevents cortical porosity.

The translational potential of this article: This study clarified the roles of Sp7 in differentiated osteoblasts in proliferarion, maturation, *Col1a1* expression, and osteocyte process formation, which are required for targeting SP7 in the development of therapies for osteoporosis.

1. Introduction

Runt related transcription factor 2 (Runx2), a member of the Runx family of transcription factors, induces the commitment of multipotent mesenchymal cells to osteoblast lineage cells and induces the proliferation of osteoblast progenitors. Sp7, which has three zinc finger motifs and belongs to the SP family of transcription factors, and Wnt signaling, together with Runx2 are required for osteoblast differentiation. After differentiation into immature osteoblasts, Runx2 regulates the expression of major bone matrix protein genes, including *Col1a1*, collagen type I alpha 2 chain (*Col1a2*), *Spp1*, integrin binding sialoprotein (*Ibsp*), *Bglap/Bglap2* [1]. Although the SP family of transcription factors bind GC-rich target sequences through the zinc finger domain, Sp7 interacts with distal-less homeobox (Dlx) and binds to the AT-rich motifs of Dlx target genes [2].

The germline deletion of *Sp7* ($Sp7^{-/-}$) results in death just after birth, and $Sp7^{-/-}$ mice completely lack osteoblasts and bone [3]. Furthermore, $Sp7^{fl/-;CAG-CreER}$ mice treated with tamoxifen, which causes the ubiquitous deletion of *Sp7* after birth, markedly reduced both bone formation and trabecular and cortical bone volumes [4]. Therefore, Sp7 is essential for osteoblast differentiation and bone formation during the embryonic stage and after birth. Moreover, *SP7* is a locus associated with osteoporosis and a rare pathogenetic locus of osteogenesis imperfecta [5]. Sp7 is expressed in both osteoblasts and hypertrophic chondrocytes, and is required for matrix metallopeptidase 13 (*Mmp13*) expression in terminal hypertrophic chondrocytes [6].

To investigate the functions of Sp7 in differentiated osteoblasts, Baek et al. generated $Sp7^{fl/-;Col1a1-Cre}$ mice, in which one *Sp7* allele was deleted in germline and the other *Sp7* allele was conditionally deleted in osteoblasts using 2.3-kb *Col1a1* Cre. In femurs, the trabecular bone volume increased, while cortical bone volume was normal. In vertebrae, the trabecular bone volume and the bone formation were reduced. The expression of *Bglap/Bglap2*, but not *Col1a1*, was reduced [7]. The same group also generated $Sp7^{fl/-;Col1a1-CreERT2}$ mice and 4-hydroxytamoxifen (4-OHT) was injected after birth. The numbers of osteoblasts, osteoclasts, and BrdU-positive cells were similar in 4-OHT treated and control mice, while the expression of *Col1a1* and *Bglap/Bglap2* was lower in 4-OHT treated mice [8]. Osteocyte anomalies were not examined in either of the mouse models. Although the sexes of the mice examined were not specified, the two mouse models indicated that the deletion of *Sp7* in osteoblasts in the *Sp7* haplodeficient state decreased vertebral trabecular bone by inhibiting osteoblast maturation, increased femoral trabecular bone via unknown mechanisms, and did not affect cortical bone volume, osteoblast proliferation, and bone resorption. Another group generated $Sp7^{OcyKO}$ mice using *Dmp1* Cre, which directs Cre expression in mature osteoblasts and osteocytes. $Sp7^{OcyKO}$ mice had porous cortical bone, fewer osteocyte processes and canaliculi, and more TUNEL-positive lacunae in the cortical bone, indicating the need for Sp7 to acquire a sufficient number of osteocyte processes [9].

Osteocytes form a dense network through their processes and canaliculi throughout bone. Reductions in the numbers of osteocyte processes and canaliculi induce osteocyte apoptosis through decreases in the supply of oxygen and nutrients to osteocytes via these processes and canaliculi [9–12]. Apoptotic osteocytes have been shown to increase the expression of TNF superfamily member 11 (*Tnfsf11*, also known as *Rankl*), which encodes a ligand for TNF receptor superfamily member 11 (Tnfrsf11a/Rank), in neighboring osteocytes and osteoblasts through the release of adenosine triphosphate (ATP), thereby promoting osteoclastogenesis and bone resorption [13–16]. Furthermore, secondary necrosis occurs in the majority of apoptotic osteocytes because scavengers cannot reach the apoptotic osteocytes imbedded in the bone matrix. Inflammatory molecules, including damage-associated molecular patterns, are released through the canaliculi to the bone surface and vascular canals in bone, leading to the production of proinflammatory cytokines that induce *Tnfsf11* expression [16–18].

Although Sp7 is essential for osteoblast differentiation, the functions of Sp7 in bone formation, bone resorption, and bone matrix protein gene expression remain unclear, and the effects of the deletion of *Sp7* on osteocytes have not been examined in previous osteoblast-specific *Sp7* knockout mice using 2.3-kb *Col1a1* Cre. Therefore, we examined $Sp7^{floxneo/floxneo}$ mice, in which *Sp7* expression was reduced to 30 % of that in wild-type mice through disturbed splicing by neo gene insertion, and osteoblast-specific knockout ($Sp7^{fl/fl;Col1a1-Cre}$) mice generated using 2.3-kb *Col1a1* EGFP-Cre transgenic mice [19]. Although the knockdown or deletion of *Sp7* in osteoblasts exerted differential effects in males and females, in long bones and vertebrae, and in trabecular and cortical bone, the results demonstrated that Sp7 inhibits the proliferation of immature osteoblasts and induces their differentiation, and that Sp7 is required for *Col1a1* expression and for acquiring a sufficient number of osteocyte processes. The reduction in the number of osteocyte processes resulted in severe cortical porosity due to the osteocyte death, which enhanced osteoclastogenesis.

2. Results

2.1. Reduced Sp7 expression in neo-inserted Sp7 floxed mice

The *Sp7* gene comprises two exons, and two major mRNAs (Types I and II) were transcribed from different transcription start sites (Supplementary Fig. 1A) [20]. This was confirmed by Cap Analysis of Gene Expression (CAGE) using RNA from wild-type calvariae (Supplementary Fig. 1B). The neo gene interposed between frts was inserted into the intron and loxp sequences in the 5' of neo and the untranslated region of exon 2 (Supplementary Fig. 1A) [6]. We initially examined neo-inserted *Sp7* floxed mice ($Sp7^{floxneo/+}$ and $Sp7^{floxneo/floxneo}$). Real-time RT-PCR analyses using the primer sets F1 and R1 in exon 1 of Type I mRNA or F2 and R2 in exon 1 of Type II mRNA showed no reduction in *Sp7* mRNA in $Sp7^{floxneo/+}$ and $Sp7^{floxneo/floxneo}$ mice compared to those in $Sp7^{+/+}$ mice, indicating that the transcriptional activities for Type I and Type II mRNA were not affected by neo gene insertion. However, real-time RT-PCR analyses using the primer sets F3 (exon 1 in Type I mRNA) and R3 (exon 2) or F4 (exon 1 in Type II) and R3 (exon 2) revealed a decrease in *Sp7* mRNA in $Sp7^{floxneo/+}$ and $Sp7^{floxneo/floxneo}$ mice compared to $Sp7^{+/+}$ mice (Supplementary Fig. 1C). Furthermore, real-time RT-PCR using the primers in exon 2 (F5 and R3) also showed a reduction in *Sp7* mRNA in $Sp7^{floxneo/floxneo}$ mice compared to $Sp7^{+/+}$ mice (Supplementary Fig. 1C). These results indicated that neo gene insertion in the intron disturbed splicing and reduced Type I and Type II *Sp7* mRNAs. Type I and Type II *Sp7* mRNAs in $Sp7^{floxneo/+}$ mice and $Sp7^{floxneo/floxneo}$ mice were approximately 60 and 30 %, respectively, of those in $Sp7^{+/+}$ mice.

Similar results were obtained in western blot analyses of $Sp7^{+/+}$, $Sp7^{floxneo/+}$, and $Sp7^{floxneo/floxneo}$ newborn limbs using the Sp7 antibody (Supplementary Figs. 1D and E). Therefore, $Sp7^{floxneo/floxneo}$ mice, in which *Sp7* mRNA is less than one-third of that in wild-type mice, are a useful model for examining the role of Sp7.

2.2. Micro-CT and gene expression analyses in $Sp7^{floxneo/floxneo}$ and $Sp7^{floxneo/floxneo;Col1a1-Cre}$ mice at 9 weeks of age

We generated $Sp7^{floxneo/floxneo;Col1a1-Cre}$ mice using 2.3-kb *Col1a1* EGFP-Cre transgenic mice [19], and compared the body weights and trabecular and cortical bone of femurs among male $Sp7^{+/+}$, $Sp7^{floxneo/+}$, $Sp7^{floxneo/floxneo}$, and $Sp7^{floxneo/floxneo;Col1a1-Cre}$ mice and between female $Sp7^{+/+}$ and $Sp7^{floxneo/floxneo}$ mice. Body weights were lower in male $Sp7^{floxneo/floxneo;Col1a1-Cre}$ mice and female $Sp7^{floxneo/floxneo}$ mice than in the respective $Sp7^{+/+}$ mice (Fig. 1A). In micro-CT analyses of males, no significant differences were observed in trabecular bone volume (BV/TV) or trabecular thickness (Tb.Th) among the four groups, while the trabecular number (Tb.N) was increased in $Sp7^{floxneo/floxneo;Col1a1-Cre}$ mice and trabecular bone mineral density (Tb.BMD) was reduced in $Sp7^{floxneo/floxneo}$ and $Sp7^{floxneo/floxneo;Col1a1-Cre}$ mice (Fig. 1B–F). In females, BV/TV and Tb.N were higher in $Sp7^{floxneo/floxneo}$ mice than in $Sp7^{+/+}$ mice, while Tb.Th and Tb.BMD were similar (Fig. 1C–G). Cortical area (CtAr/TtAr), cortical thickness (Ct.Th), and cortical (Ct) BMD were lower in male $Sp7^{floxneo/floxneo}$ and $Sp7^{floxneo/floxneo;Col1a1-Cre}$ mice and female $Sp7^{floxneo/floxneo}$ mice than in the respective $Sp7^{+/+}$ mice (Fig. 1D, E, H, I). The periosteal perimeter (Ps.Pm) of cortical bone in male $Sp7^{floxneo/floxneo;Col1a1-Cre}$ mice and the endosteal perimeter (Es.Pm) in male $Sp7^{floxneo/floxneo;Col1a1-Cre}$ mice and female $Sp7^{floxneo/floxneo}$ mice were higher than those in the respective $Sp7^{+/+}$ mice (Fig. 1H and I). Body weights and all parameters in the micro-CT analysis were similar in $Sp7^{floxneo/+}$ and $Sp7^{+/+}$ male mice (Fig. 1).

The expression of the osteoblast marker genes, *Tnfsf11,* and TNF receptor superfamily member 11b (*Tnfrsf11b*, also known as *Opg*), which is a decoy receptor for Tnfsf11, was compared using RNA from the osteoblast-enriched fraction in male $Sp7^{floxneo/+}$, $Sp7^{floxneo/floxneo}$, and $Sp7^{neo/neo;Col1a1-Cre}$ mice (Supplementary Fig. 2A). The expression of *Sp7* was lower in $Sp7^{floxneo/floxneo}$ mice and $Sp7^{floxneo/floxneo;Col1a1-Cre}$ mice, but the expression of *Spp1* and *Tnfsf11* was higher in $Sp7^{floxneo/floxneo;Col1a1-Cre}$ mice than in $Sp7^{floxneo/+}$ mice, *Tnfsf11* expression in $Sp7^{floxneo/floxneo;Col1a1-Cre}$ mice was higher than in $Sp7^{floxneo/floxneo}$ mice, and the expression of the other genes examined was similar among the three groups (Supplementary Fig. 2A). The expression of osteocyte marker genes, including dentin matrix acidic phosphoprotein 1 (*Dmp1*) and sclerostin (*Sost*), using the osteocyte-enriched fraction in male mice was markedly lower in $Sp7^{floxneo/floxneo}$ and $Sp7^{floxneo/floxneo;Col1a1-Cre}$ mice than in $Sp7^{floxneo/+}$ mice (Supplementary Fig. 2B).

2.3. Micro-CT analysis and the serum markers for bone formation and resorption in $Sp7^{fl/fl;Col1a1-Cre}$ mice at 10 weeks of age

The neo gene was deleted by mating $Sp7^{floxneo/+}$ mice with CAG-Flp transgenic mice to generate and $Sp7^{fl/+}$ and $Sp7^{fl/fl}$ mice. The body weights and all trabecular and cortical bone parameters on micro-CT were similar between the $Sp7^{fl/+}$ and $Sp7^{fl/fl}$ mice (Supplementary Figs. 3A–E). Furthermore, the expression of *Sp7*, the osteoblast marker genes, *Tnfsf11,* and *Tnfrsf11b* in the osteoblast-enriched fraction, and osteocyte marker genes in the osteocyte-enriched fraction were similar (Supplementary Figs. 3F and G).

To examine Sp7 functions specifically in differentiated osteoblasts, $Sp7^{fl/+}$ and $Sp7^{fl/fl}$ mice were mated with 2.3-kb *Col1a1* EGFP-Cre transgenic mice to generate $Sp7^{fl/fl;Col1a1-Cre}$ mice. $Sp7^{fl/fl;Col1a1-Cre}$ mice were compared with the $Sp7^{fl/+}$ and $Sp7^{fl/fl}$ littermates as the control, because there were no differences between the $Sp7^{fl/+}$ and $Sp7^{fl/fl}$ littermates (Supplementary Fig. 3). Body weights were similar in $Sp7^{fl/fl;Col1a1-Cre}$ mice and the control in both sexes (Fig. 2A). In micro-CT analyses of femoral trabecular bone, BV/TV and Tb.N were higher and Tb.BMD was lower in female $Sp7^{fl/fl;Col1a1-Cre}$ mice than in the control, while these parameters in male $Sp7^{fl/fl;Col1a1-Cre}$ mice were similar to those in the control (Fig. 2B, C, F, G). CtAr/TtAr, Ct.Th, and Ct.BMD were lower and Ps.Pm was higher in both male and female $Sp7^{fl/fl;Col1a1-Cre}$ mice and Es.Pm was higher in female $Sp7^{fl/fl;Col1a1-Cre}$ mice than in the respective controls (Fig. 2D, E, H, I). As the cortical bone was porous in $Sp7^{floxneo/floxneo}$, $Sp7^{floxneo/flox\ neo;Col1a1-Cre}$, and $Sp7^{fl/fl;Col1a1-Cre}$ mice (Fig. 1D, E, 2D, E), the level of the cortical pososity was compared at the mid-diaphysis of male femurs using high-resolution micro-CT. The cortical pososity in $Sp7^{floxneo/floxneo}$ mice was more severe than in $Sp7^{floxneo/+}$ mice, that in $Sp7^{floxneo/floxneo;Col1a1-Cre}$ mice was more severe than in $Sp7^{floxneo/floxneo}$ mice, and that in $Sp7^{fl/fl;Col1a1-Cre}$ mice was more severe than in $Sp7^{fl/fl}$ mice (Fig. 2J–M).

Because the male and female vertebrae were examined using different micro-CT systems (Skyscan1176 for males and R_mCT for females), the data could not be compared between males and females. In male lumbar vertebrae, BV/TV and Tb.BMD in $Sp7^{fl/fl;Col1a1-Cre}$ mice were lower than those in the control ($Sp7^{fl/+}$ and $Sp7^{fl/fl}$) (Fig. 3A and B). In females, BV/TV, Tb.Th, and Tb.N in lumbar vertebrae were lower in $Sp7^{fl/fl;Col1a1-Cre}$ mice than in the control ($Sp7^{fl/fl}$), whereas Tb.BMD was similar (Fig. 3C and D).

The serum marker for bone formation, total procollagen type 1 N-terminal propeptide (P1NP), was similar in female $Sp7^{fl/fl;Col1a1-Cre}$ mice and controls, whereas that for bone resorption, tartrate-resistant acid phosphatase 5b (TRAP5b), was higher in the former (Fig. 3E).

2.4. Bone histomorphometric analyses in female $Sp7^{fl/fl;Col1a1-Cre}$ mice at 10 weeks of age

Bone histomorphometric analyses were performed using tibiae, vertebrae, and femoral cortical bone from female $Sp7^{fl/fl}$ and $Sp7^{fl/fl;Col1a1-Cre}$ mice at 10 weeks of age. In tibiae, osteoblast parameters, including the osteoid surface, osteoblast surface, and osteoblast number, and the mineral apposition and bone formation rate were higher in $Sp7^{fl/fl;Col1a1-Cre}$ mice than in $Sp7^{fl/fl}$ mice (Fig. 4B). In contrast, these parameters and osteoid thickness in vertebrae were lower in $Sp7^{fl/fl;Col1a1-Cre}$ mice than in $Sp7^{fl/fl}$ mice (Fig. 4D). Osteoclast parameters, including the osteoclast surface, osteoclast number, and eroded surface, in trabecular bone in tibiae and vertebrae were similar between $Sp7^{fl/fl;Col1a1-Cre}$ and $Sp7^{fl/fl}$ mice (Fig. 4B and D). In femoral cortical bone, the mineral apposition rate and bone formation rate in the periosteum and endosteum were similar between $Sp7^{fl/fl;Col1a1-Cre}$ mice and $Sp7^{fl/fl}$ mice, while the mineralizing surface in the periosteum, but not in the endosteum, was higher in $Sp7^{fl/fl;Col1a1-Cre}$ mice than in $Sp7^{fl/fl}$ mice (Fig. 4E–K).

2.5. Histological analyses of the femurs in male $Sp7^{fl/fl;Col1a1-Cre}$ mice by BrdU labeling and the staining with TUNEL, Safranin O, and TRAP

The proliferation of osteoblastic cells was examined by BrdU labeling at three weeks of age. The frequency of BrdU-positive osteoblastic cells was higher in $Sp7^{fl/fl;Col1a1-Cre}$ mice than in $Sp7^{fl/fl}$ mice (Fig. 5A–E). Furthermore, the frequencies of BrdU-positive osteoblastic cells in the two female $Sp7^{fl/fl;Col1a1-Cre}$ mice (19.7 % and 20.0 %) were similar to those in male $Sp7^{fl/fl;Col1a1-Cre}$ mice. The apoptosis of osteoblasts and osteocytes was examined using the TUNEL assay. The frequency of TUNEL-positive osteoblastic cells in the endosteum at the metaphysis was similar between $Sp7^{fl/fl}$ and $Sp7^{fl/fl;Col1a1-Cre}$ mice, whereas that of TUNEL-positive lacunae increased in both trabecular and cortical bones and was higher in cortical bone than in trabecular bone (Fig. 5F–R). Since calcified cartilage accumulated below the growth plate in $Sp7^{fl/-;CAG-CreER}$ mice treated with tamoxifen [4], the cartilage matrix was stained with safranin O. The safranin O-positive area below the growth plate was similar between $Sp7^{fl/fl}$ and $Sp7^{fl/fl;Col1a1-Cre}$ mice, indicating that the resorption of bone and cartilage similarly occurred in the

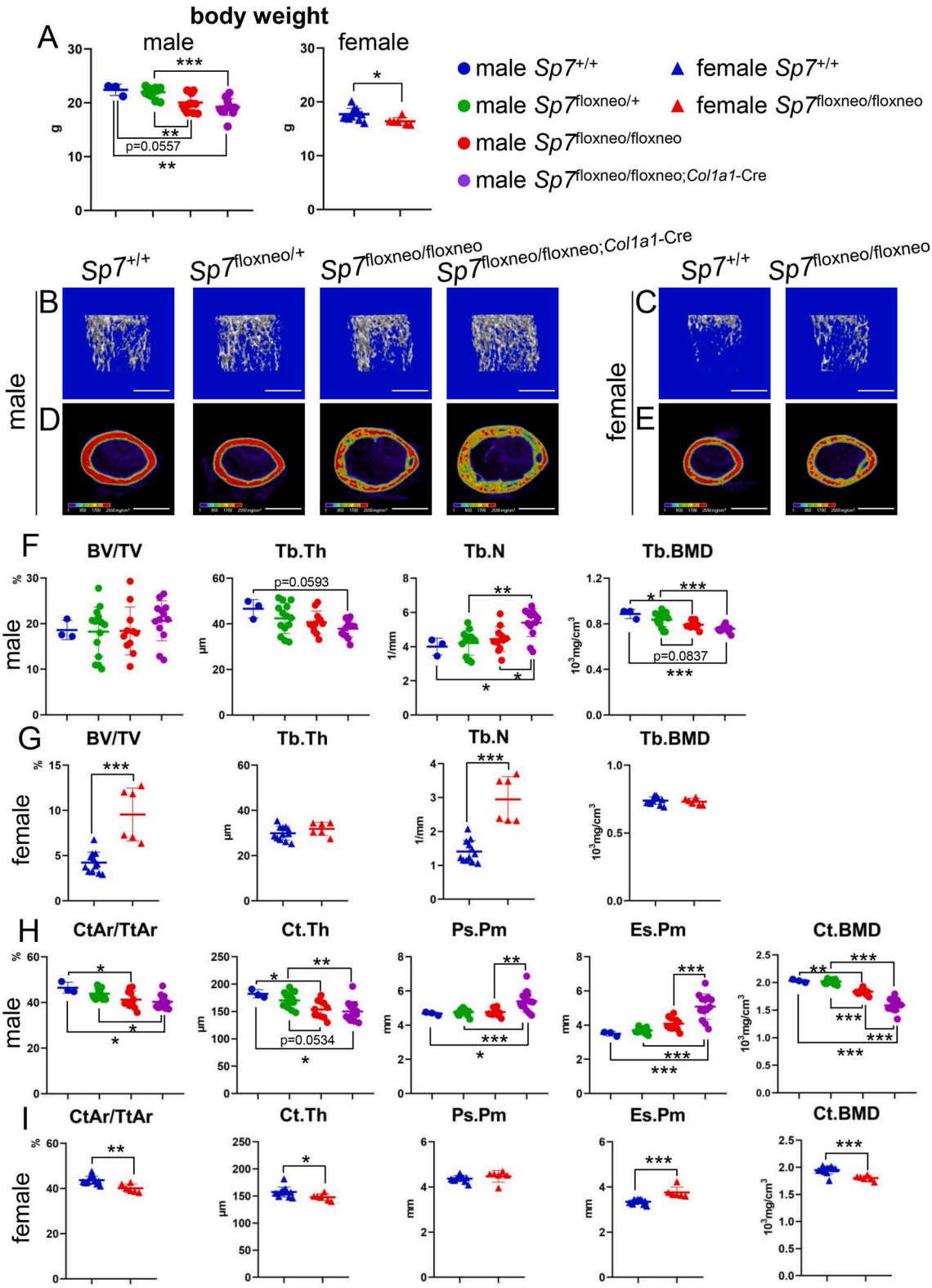

Figure 1. Micro-CT analyses of $Sp7^{+/+}$, $Sp7^{floxneo/+}$, $Sp7^{floxneo/floxneo}$, and $Sp7^{floxneo/floxneo;Col1a1-Cre}$ mice at 9 weeks of age (A) Body weights of male $Sp7^{+/+}$, $Sp7^{floxneo/+}$, $Sp7^{floxneo/floxneo}$, and $Sp7^{floxneo/floxneo;Col1a1-Cre}$ mice and female $Sp7^{+/+}$ and $Sp7^{floxneo/floxneo}$ mice (B–E) Three-dimensional trabecular bone architecture of the distal femoral metaphysis (B, C) and images of cortical bone at the mid-diaphysis of the femur (D, E) in male (B, D) and female (C, E) mice. Scale bars: 1 mm. (F–I) Quantification of trabecular bone (F, G) and cortical bone (H, I) parameters in male $Sp7^{+/+}$, $Sp7^{floxneo/+}$, $Sp7^{floxneo/floxneo}$, and $Sp7^{floxneo/floxneo;Col1a1-Cre}$ mice (F, H) and female $Sp7^{+/+}$ and $Sp7^{floxneo/floxneo}$ mice (G, I). These parameters include trabecular bone volume (bone volume/tissue volume, BV/TV), trabecular thickness (Tb.Th), trabecular number (Tb.N), trabecular bone mineral density (Tb.BMD), cortical area (CtAr/TtAr), cortical thickness (Ct.Th), periosteal perimeter (Ps.Pm), endosteal perimeter (Es.Pm), and cortical bone mineral density (Ct.BMD). n = 3 (male $Sp7^{+/+}$), n = 14 (male $Sp7^{floxneo/+}$), n = 12 (male $Sp7^{floxneo/floxneo}$), n = 13 (male $Sp7^{floxneo/floxneo;Col1a1-Cre}$), n = 12 (female $Sp7^{+/+}$), and n = 6 (female $Sp7^{floxneo/floxneo}$).

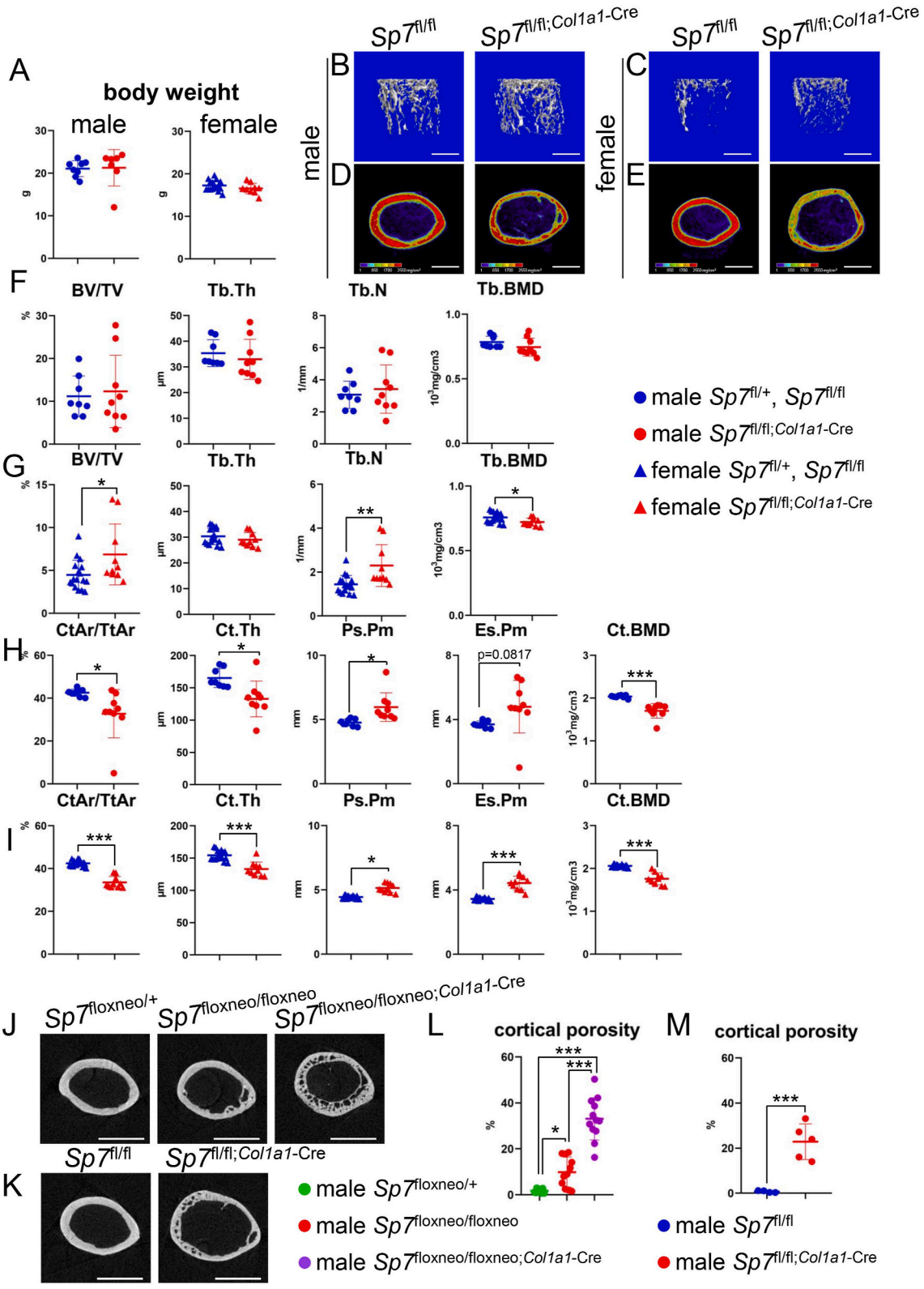

Figure 2. Micro-CT analyses of femurs in $Sp7^{fl/fl;Col1a1-Cre}$ mice without neo at 10 weeks of age (A) Body weight of male and female $Sp7^{fl/fl;Col1a1-Cre}$ and the control ($Sp7^{fl/+}$ and $Sp7^{fl/fl}$) mice. (B–E) Three-dimensional trabecular bone architecture of the distal femoral metaphysis (B, C) and images of the cortical bone at the mid-diaphysis in the femurs (D, E) of male (B, D) and female (C, E) $Sp7^{fl/fl}$ and $Sp7^{fl/fl;Col1a1-Cre}$ mice. Scale bars: 1 mm. (F–I) Quantification of trabecular bone (F, G) and cortical bone (H, I) parameters in male (F, H) and female (G, I) $Sp7^{fl/fl;Col1a1-Cre}$ and the control ($Sp7^{fl/+}$ and $Sp7^{fl/fl}$) mice. n = 8 (4 male $Sp7^{fl/+}$ and 4 $Sp7^{fl/fl}$), n = 7 (male $Sp7^{fl/fl;Col1a1-Cre}$), n = 17 (7 female $Sp7^{fl/+}$ and 10 $Sp7^{fl/fl}$), and n = 10 (female $Sp7^{fl/fl;Col1a1-Cre}$). (J–M) High resolution micro-CT images of cortical bone at the mid-diaphysis in male femurs (J, K) and the quantification of cortical porosity (L, M). The percentage of the pore area in the cortical area is shown. n = 14 ($Sp7^{floxneo/+}$), n = 11 ($Sp7^{floxneo/floxneo}$), n = 12 ($Sp7^{floxneo/floxneo;Col1a1-Cre}$), n = 4 ($Sp7^{fl/fl}$), and n = 5 ($Sp7^{fl/fl;Col1a1-Cre}$).

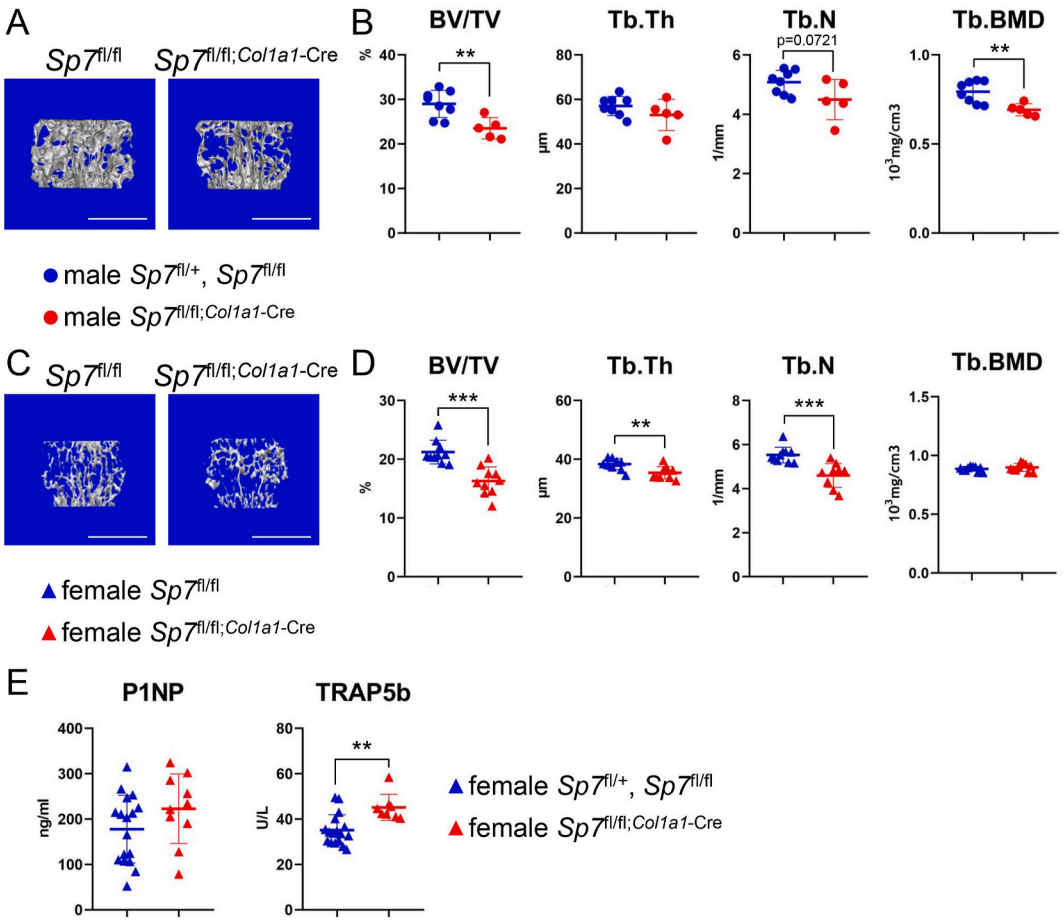

Figure 3. Micro-CT analysis of vertebrae and the serum markers for bone formation and resorption in $Sp7^{fl/fl;Col1a1-Cre}$ mice at 10 weeks of age (A–D) Three-dimensional trabecular bone architecture of the first lumbar vertebra (A, C) and the quantification of BV/TV, Tb.Th, Tb.N, and Tb.BMD (B, D) in male (A, B) and female (C, D) $Sp7^{fl/fl;Col1a1-Cre}$ and the control (male $Sp7^{fl/+}$ and $Sp7^{fl/fl}$ and female $Sp7^{fl/fl}$) mice. Scale bars: 1 mm. n = 8 (male 4 $Sp7^{fl/+}$ and 4 $Sp7^{fl/fl}$), n = 5 (male $Sp7^{fl/fl;Col1a1-Cre}$), n = 10 (female $Sp7^{fl/fl}$), and n = 10 (female $Sp7^{fl/fl;Col1a1-Cre}$). Vertebrae from males and females were analyzed using different micro-CT systems. (E) Serum levels of P1NP and TRAP5b in female $Sp7^{fl/fl;Col1a1-Cre}$ and the control ($Sp7^{fl/+}$ and $Sp7^{fl/fl}$) mice. n = 17 (7 $Sp7^{fl/+}$ and 10 $Sp7^{fl/fl}$) and n = 8 ($Sp7^{fl/fl;Col1a1-Cre}$).

primary spongiosa (Fig. 5S–U). The accumulation of calcified cartilage in $Sp7^{fl/-;CAG-CreER}$ mice treated with tamoxifen is likely due to the impaired degradation of the cartilage matrix by Mmp13 [4,6]. As osteocyte apoptosis has been shown to enhance bone resorption [16], TRAP-positive osteoclasts were counted. The number of TRAP-positive osteoclasts was similar between $Sp7^{fl/fl}$ and $Sp7^{fl/fl;Col1a1-Cre}$ mice in the trabecular bone, whereas it was markedly higher in $Sp7^{fl/fl;Col1a1-Cre}$ mice than in $Sp7^{fl/fl}$ mice in the cortical bone (Fig. 5V–Z″).

2.6. Histological analysis of canaliculi and Sost expression and gene expression analysis in $Sp7^{fl/fl;Col1a1-Cre}$ mice at 10 weeks of age

The number of canaliculi per osteocyte in both femoral trabecular and cortical bone was lower in male $Sp7^{fl/fl;Col1a1-Cre}$ mice than in $Sp7^{fl/fl}$ mice and the lacunocanalicular network was severely disorganized (Fig. 6A–H, Q). Sost is expressed in osteocytes and antagonizes canonical Wnt signaling through binding to Wnt co-receptor low density lipoprotein receptor-related ptotein (Lrp) 5 and Lrp6 [11,21,22]. The number of Sost-positive osteocytes in both femoral trabecular and cortical bone was lower in male $Sp7^{fl/fl;Col1a1-Cre}$ mice than in $Sp7^{fl/fl}$ mice (Fig. 6I–P, R).

Since male mice were histologically analyzed by perfusion fixation, RNA samples of the osteoblast and osteocyte fractions were collected from female tibiae and the mRNA expression in $Sp7^{fl/fl;Col1a1-Cre}$ mice was compared with that in $Sp7^{fl/+}$ and $Sp7^{fl/fl}$ mice. The expression of *Sp7*, *Col1a1*, and *Bglap/Bglap2* was lower, whereas that of *Spp1* and *Tnfsf11* and the ratio of *Tnfrsf11/Tnfrsf11b* in the osteoblast fraction were higher in $Sp7^{fl/fl;Col1a1-Cre}$ mice than in the controls (Fig. 7A). The expression of all osteocyte marker genes in the osteocyte fraction, including *Dmp1*, *Sost*, phosphate regulating endopeptidase X-linked (*Phex*), fibroblast growth factor 23 (*Fgf23*), and matrix extracellular phosphoglycoprotein (*Mepe*), was markedly lower in $Sp7^{fl/fl;Col1a1-Cre}$ mice than in the controls (Fig. 7B). Although Ostn was previously reported to be responsible for the reduction in osteocyte processes [9], *Ostn* expression in the osteoblast fraction was higher in $Sp7^{fl/fl;Col1a1-Cre}$ mice than in the control (Fig. 7A). *Ostn* expression in the osteocyte fraction was similar in $Sp7^{fl/fl;Col1a1-Cre}$ mice and control mice (Fig. 7B). *Ostn* expression was also examined in osteoblast-specific *Sp7* (*Col1a1-Sp7*) transgenic mice under the control of the 2.3-kb *Col1a1* promoter. *Ostn* expression in both the osteoblast and osteocyte fractions was similar in male *Col1a1-Sp7* transgenic mice and the male wild-type littermates (Fig. 7C). Moreover, *Sp7* overexpression in osteoblastic MC3T3-E1 cells failed to induce *Ostn* (Fig. 7D).

2.7. Histological analysis of osteoblasts in the morphology and Col1a1 expression in $Sp7^{fl/fl;Col1a1-Cre}$ mice at 3 weeks of age

As *Col1a1* expression was reduced in $Sp7^{fl/fl;Col1a1-Cre}$ mice (Fig. 7A), the protein expression of Sp7, Runx2, and Col1a1 and the morphology of osteoblasts were compared between $Sp7^{fl/fl}$ and $Sp7^{fl/fl;Col1a1-Cre}$ mice

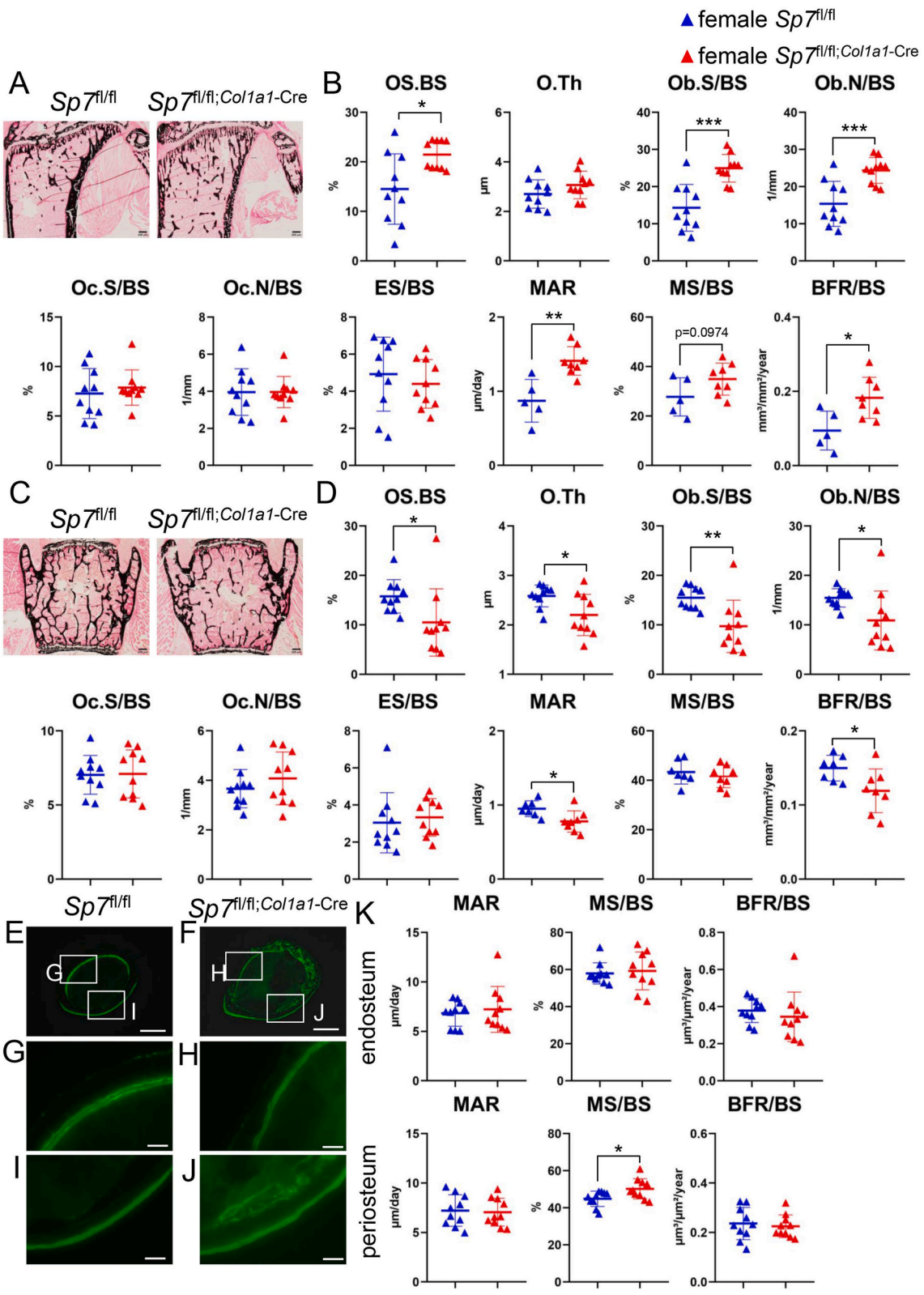

Figure 4. Bone histomorphometric analyses of trabecular bone in tibiae, vertebrae, and femoral cortical bone in female *Sp7*$^{fl/fl}$ and *Sp7*$^{fl/fl;Col1a1-Cre}$ mice at 10 weeks of age (A–D) von Kossa staining of tibiae (A) and lumber vertebrae (C), and trabecular bone parameters, including the osteoid surface (OS/BS), osteoid thickness (O.Th), osteoblast surface (Ob.S/BS), osteoblast number (Ob.N/BS), osteoclast surface (Oc.S/BS), osteoclast number (Oc.N/BS), eroded surface (ES/BS), mineral apposition rate (MAR), mineralizing surface (MS/BS), and bone formation rate (BFR/BS) in tibiae (B) and vertebrae (D). BS, bone surface. Scale bars: 0.2 mm. (E–K) Dynamic bone histomorphometric analyses of cortical bone. Cross-sections of the mid-diaphyses of femurs were analyzed. G and H show the endosteum and I and J show the periosteum. The boxed regions in E and F are magnified in G and I and in H and J, respectively. Scale bars: 0.5 mm (E, F) and 0.1 mm (G–J). MAR, MS/BS, and BFR/BS in the endosteum and periosteum are shown in K. n = 10 (*Sp7*$^{fl/fl}$) and n = 10 (*Sp7*$^{fl/fl;Col1a1-Cre}$).

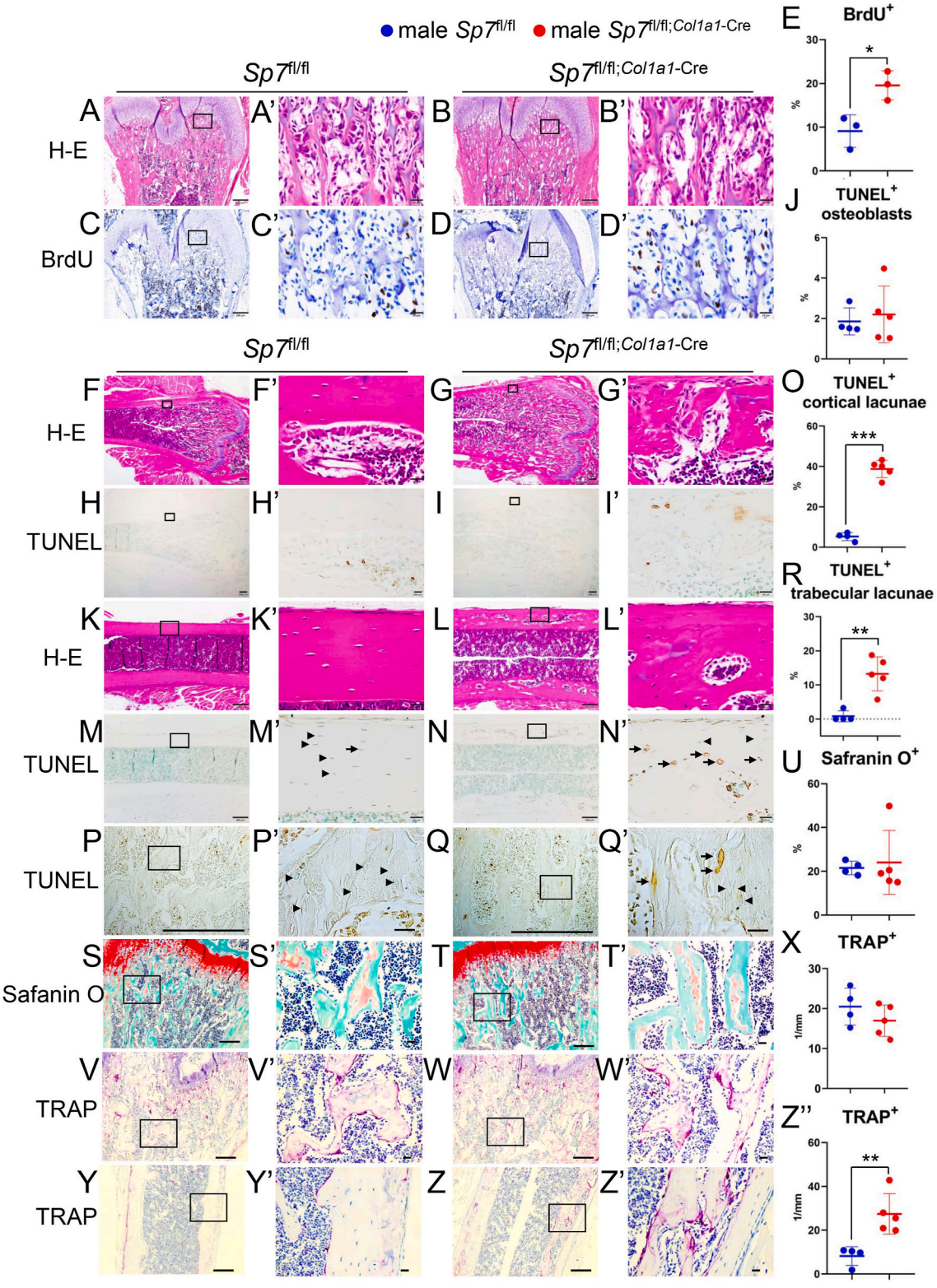

(caption on next page)

Figure 5. Proliferation of osteoblastic cells, apoptosis of osteoblasts and osteocytes, and bone resorption in the femurs of male $Sp7^{fl/fl}$ and $Sp7^{fl/fl;Col1a1-Cre}$ mice (A–E) Proliferation of osteoblastic cells in trabecular bone of $Sp7^{fl/fl}$ and $Sp7^{fl/fl;Col1a1-Cre}$ mice at 3 weeks of age. A and B, H-E staining. C and D, BrdU staining, which was counterstained with hematoxylin. E, Frequency of BrdU-positive cells in the region shown in C′ and D'. n = 3 ($Sp7^{fl/fl}$ mice) and n = 3 ($Sp7^{fl/fl;Col1a1-Cre}$ mice). (F–R) Apoptosis of osteoblasts and osteocytes in $Sp7^{fl/fl}$ and $Sp7^{fl/fl;Col1a1-Cre}$ mice at 10 weeks of age. F–J, H-E (F, G), and TUNEL (H, I) staining of metaphyseal cortical bone and the frequency of TUNEL-positive osteoblasts in the endosteum (J). K–O, H-E (K, L), and TUNEL (M, N) staining of cortical bone at the mid-diaphysis and the frequency of TUNEL-positive lacunae in cortical bone (O). P–R, TUNEL staining of trabecular bone (P, Q) and the frequency of TUNEL-positive lacunae in trabecular bone (R). Arrows show TUNEL-positive lacunae and arrowheads show TUNEL-negative osteocytes in M′, N′, P′, and Q'. The number of TUNEL-positive lacunae and TUNEL-negative osteocytes were counted, and the frequency of TUNEL-positive lacunae was calculated. TUNEL stained sections were counterstained with methyl green. (S–Z) Safranin O staining of trabecular bone (S, T) and TRAP staining of trabecular bone (V, W) and cortical bone (Y, Z) in $Sp7^{fl/fl}$ and $Sp7^{fl/fl;Col1a1-Cre}$ mice at 10 weeks of age. The ratio of the safranin O-positive area to the total bone area is shown in U, and the number of TRAP-positive cells in the trabecular and cortical bones is shown in X and Z″, respectively. n = 4 ($Sp7^{fl/fl}$) and n = 5 ($Sp7^{fl/fl;Col1a1-Cre}$). Boxed regions in A–D, F, G, H, I, K, L, M, N, P, Q, S, T, V, W, Y and Z were magnified in A' –D′, F′, G′, H′, I′, K′, L′, M′, N′, P′, Q′, S′, T′, V′, W′, Y'and Z′, respectively. Scale bars: 200 μm (A–D, F, G, H, I, K, L, M, N, P, Q, S, T, V, W, Y and Z), 20 μm (A′–D′, F′, G′, H′, I′, K′, L′, M′, N′, P′, Q′, S′, T′, V′, W′, Y'and Z′). (For interpretation of the references to color in this figure legend, the reader is referred to the Web version of this article.)

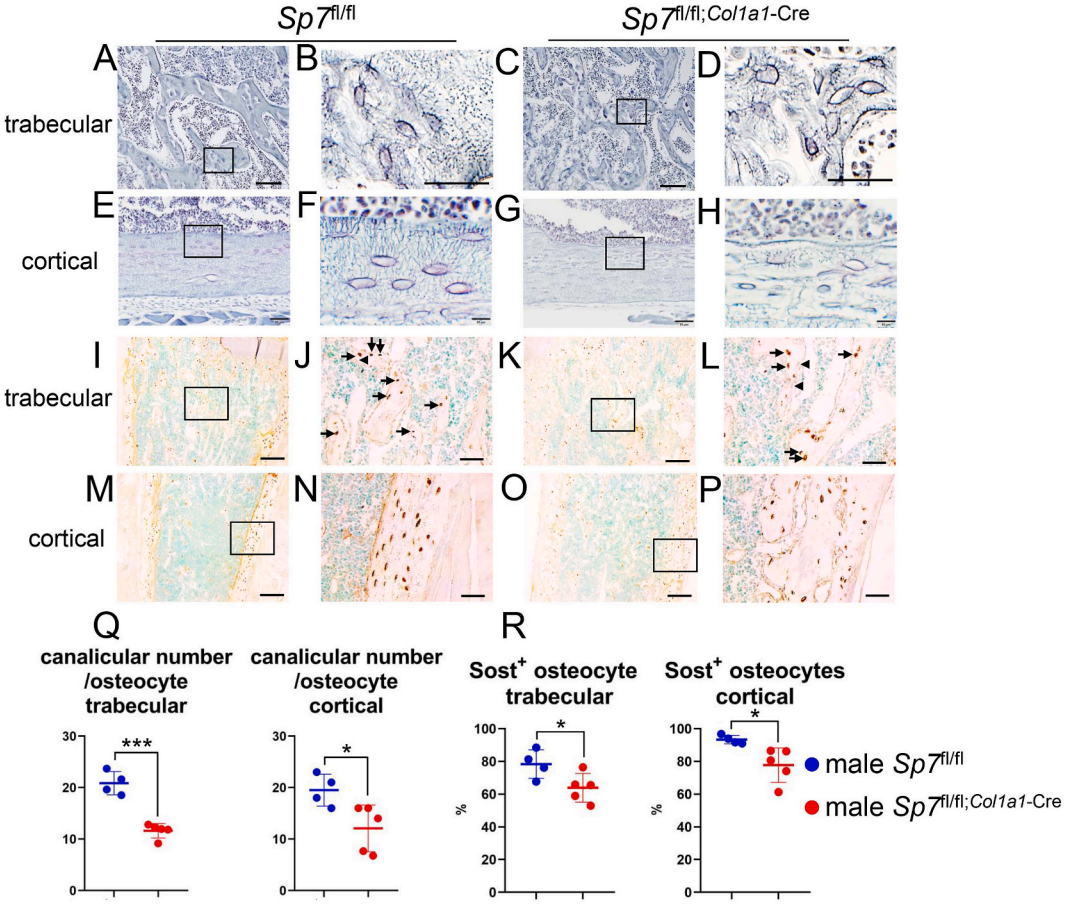

Figure 6. Canalicular staining and immunohistochemical analysis of Sost in femoral bone of male Sp7fl/fl and Sp7fl/fl;Col1a1-Cre mice at 10 weeks of age. (A–P) Canalicular staining (A–H) and immunostaining using an anti-Sost antibody (I–P) in trabecular bone (A–D, I–L) and cortical bone (E–H, M—P) of $Sp7^{fl/fl}$ (A, B, E, F, I, J, M, N) and $Sp7^{fl/fl;Col1a1-Cre}$ (C, D, G, H, K, L, O, P) mice. The boxed regions in A, C, E, G, I, K, M, and O are magnified in B, D, F, H, J, L, N, and P, respectively. The average number of canaliculi in one osteocyte was counted (Q), and the percentage of Sost-positive osteocytes was counted (R) in the trabecular and cortical bone.. n = 4 ($Sp7^{fl/fl}$) and n = 5 ($Sp7^{fl/fl;Col1a1-Cre}$). Arrows show Sost-positive osteocytes and arrowheads show Sost-negative osteocytes in J and L. The sections were then counterstained with methyl green. Scale bars: 200 μm (A, C, E, G, I, K, M, and O); 50 μm (B, D, F, H, J, L, N, and P). (For interpretation of the references to color in this figure legend, the reader is referred to the Web version of this article.)

(Fig. 8). Two types of Sp7-positive cells were observed in $Sp7^{fl/fl}$ mice. Sp7-positive cuboidal osteoblasts with a large amount of cytoplasm, located on the surface of the bone, strongly reacted with the Col1a1 antibody in the trabecular bone (Fig. 8B', F′, N′) and cortical bone (Fig. 8Q', S′, W′). Sp7-positive flattened preosteoblasts with a small amount of cytoplasm, which were located on the bone marrow side of osteoblasts, were clealy discriminated from the osteoblasts on the cortical bone and weakly reacted with the Col1a1 antibody (Fig. 8Q', S′, W′). Osteoblasts in $Sp7^{fl/fl;Col1a1-Cre}$ mice were negative for Sp7, less cuboidal than those in $Sp7^{fl/fl}$ mice, and strongly reacted with the Col1a1 antibody in the trabecular bone (Fig. 8D', H′, P′) and cortical bone (Fig. 8R', T′, X′). Flattened preosteoblasts in $Sp7^{fl/fl}$ and $Sp7^{fl/fl;Col1a1-Cre}$ mice reacted similarly to anti-Sp7 antibody (Fig. 8S', T′). Since Runx2 is an upstream transcription factor of Sp7 [1], deletion of *Sp7* in osteoblasts did not affect its expression in the trabecular bone (Fig. 8J', L′) and cortical bone (Fig. 8U', V'). Therefore, deletion of *Sp7* in osteoblasts reduced the amount of Col1a1 in osteoblasts.

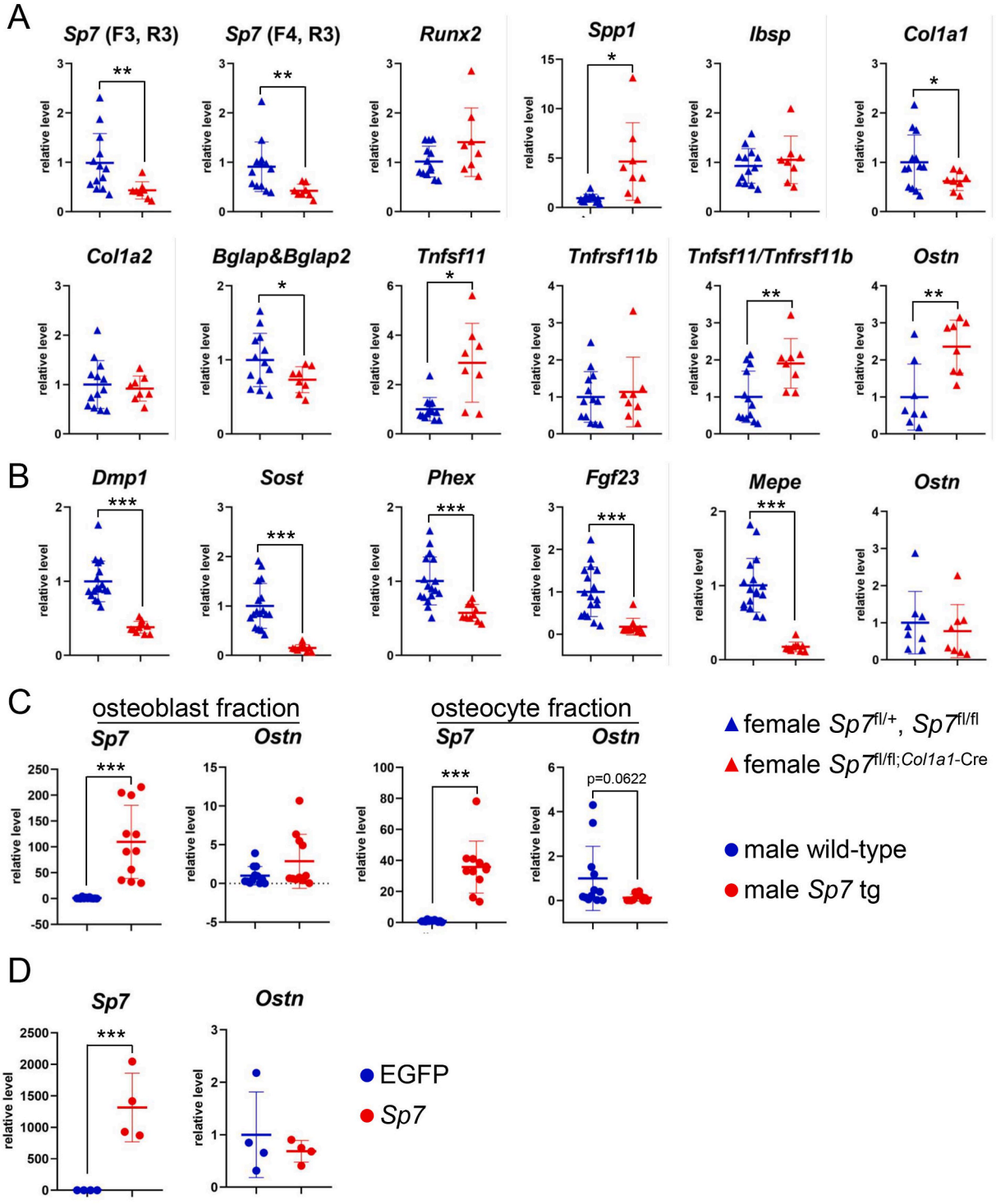

Figure 7. Real-time RT-PCR analyses of osteoblast and osteocyte marker genes, *Tnfsf11*, *Tnfrsf11b*, and *Ostn* (A, B) Real-time RT-PCR analysis of the osteoblast marker genes, *Tnfsf11*, *Tnfrsf11b*, and *Ostn* (A) and osteocyte marker genes and *Ostn* (B). RNA was extracted from the osteoblast fraction (A) and osteocyte fraction (B) of tibiae in female Sp7fl/fl;Col1a1-Cre and the control ($Sp7^{fl/+}$ and $Sp7^{fl/fl}$) mice at 10 weeks of age. The values of $Sp7^{fl/+}$ and $Sp7^{fl/fl}$ mice were defined as 1 and relative levels are shown. n = 17 (7 $Sp7^{fl/+}$ and 10 $Sp7^{fl/fl}$) and n = 10 ($Sp7^{fl/fl;Col1a1-Cre}$). (C) *Sp7* and *Ostn* expression in osteoblast and osteocyte fractions from the tibiae in male wild-type and *Col1a1-Sp7* transgenic (tg) mice at 14 weeks of age. The values of wild-type mice were defined as 1 and relative levels are shown. n = 11 (wild-type) and n = 11 (*Sp7* tg). (D) MC3T3-E1 cells were transfected with either pME18-EGFP or pME18-*Sp7*. The values of pME18-EGFP were defined as 1 and relative levels are shown. n = 4 (pME18-EGFP) and n = 4 (pME18-*Sp7*). Similar results were obtained in three independent experiments, and representative data are shown.

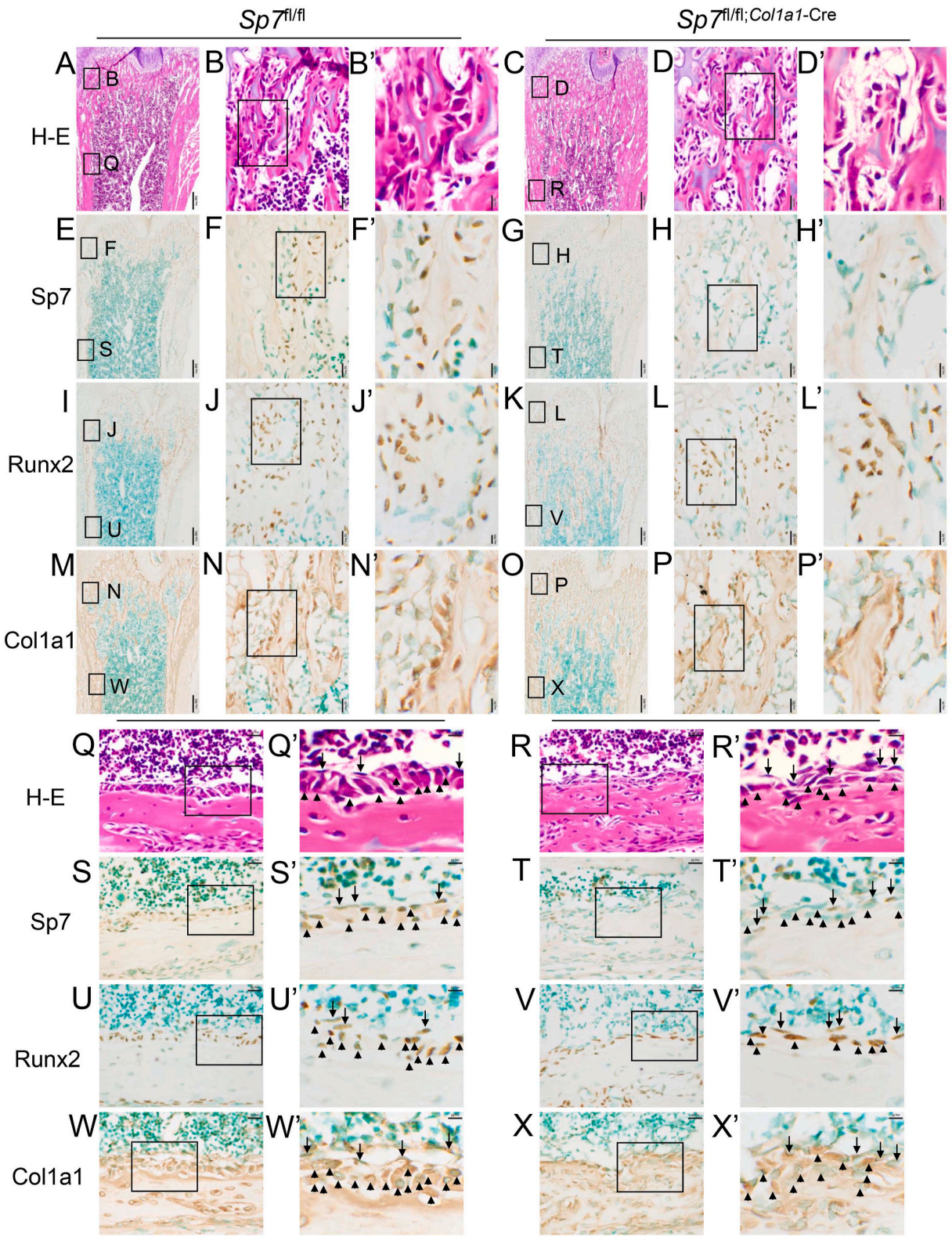

Figure 8. Histological analyses of femurs in $Sp7^{fl/fl}$ and $Sp7^{fl/fl;Col1a1-Cre}$ mice at three weeks of age H-E staining (A–D, Q, R) and immunohistochemical analyses using anti-Sp7 (E–H, S, T), anti-Runx2 (I–L, U, V), and anti-Col1a1 (M–P, W, X) antibodies in the femoral trabecular (A–P) and cortical bone (Q–X) of $Sp7^{fl/fl}$ (A, B, E, F, I, J, M, N, Q, S, U, and W) and $Sp7^{fl/fl;Col1a1-Cre}$ (C, D, G, H, K, L, O, P, R, T, V, and X) mice. Sections were counterstained with methyl green. The boxed regions in A, C, E, G, I, K, M, and O are magnified in B and Q, D and R, F and S, H and T, J and U, L and V, N and W, and P and X, respectively. B, D, F, H, J, L, N, and P–X are magnified in B′, D′, F′, H′, J′, L′, N′, and P′–X′, respectively. The pictures in Q–X were rotated 90°. Arrows show preosteoblasts, and arrowheads show osteoblasts (Q′–X′). Six male $Sp7^{fl/fl}$ mice and three male and two female $Sp7^{fl/fl;Col1a1-Cre}$ mice were analyzed and similar results were obtained. Representative data are presented here. Scale bars: 200 μm (A, C, E, G, I, K, M, and O), 20 μm (B, D, F, H, J, L, N, and P–X), and 5 μm (B′, D′, F′, H′, J′, L′, N′, and P′–X′). (For interpretation of the references to color in this figure legend, the reader is referred to the Web version of this article.)

2.8. Regulation of Col1a1 expression, osteoblastogenesis, and osteoclastogenesis by Sp7

Because EGFP expression in 2.3-kb *Col1a1* promoter EGFP-Cre transgenic mice reflects endogenous *Col1a1* expression [19], it was compared between $Sp7^{fl/+;Col1a1-Cre}$ and $Sp7^{fl/fl;Col1a1-Cre}$ newborn femurs. EGFP intensity was weaker in $Sp7^{fl/fl;Col1a1-Cre}$ mice than in $Sp7^{fl/+;Col1a1-Cre}$ mice (Supplementary Figs. 4A–D). Real-time RT-PCR analysis showed that the expression of *Sp7* and EGFP in newborn limbs was lower in $Sp7^{fl/fl;Col1a1-Cre}$ mice than in $Sp7^{fl/+;Col1a1-Cre}$ mice (Supplementary Fig. 4E). Furthermore, overexpression of *Sp7* in primary osteoblasts induced *Col1a1* expression (Supplementary Fig. 4F). These results suggest that Sp7 controls *Col1a1* expression, at least in part, through regulation of the 2.3-kb *Col1a1* promoter. Alkaline phosphatase (ALP) and von Kossa staining represent osteoblast differentiation at the early and late stages, respectively. ALP staining was stronger and von Kossa staining was weaker in $Sp7^{fl/fl;Col1a1-Cre}$ mice than in $Sp7^{fl/fl}$ mice, indicating that the number of immature osteoblasts increased among $Sp7^{fl/fl;Col1a1-Cre}$ primary osteoblasts and osteoblast maturation was inhibited (Supplementary Figs. 4G–J). In a co-culture of bone marrow-derived monocyte/macrophage lineage cells (BMMs) from wild-type mice with primary osteoblasts from $Sp7^{fl/fl}$ or $Sp7^{fl/fl;Col1a1-Cre}$ mice, the number of multinucleated osteoclasts was higher and the bone resorption area (pit area) was larger in $Sp7^{fl/fl;Col1a1-Cre}$ mice than in $Sp7^{fl/fl}$ mice (Supplementary Fig. 4K–N). These results suggest that deletion of *Sp7* in osteoblasts increases the number of immature osteoblasts, inhibits osteoblast maturation, and promotes osteoclastogenesis *in vitro*.

3. Discussion

Knockdown of *Sp7* ($Sp7^{floxneo/floxneo}$) in germline or osteoblast-specific *Sp7* deletion ($Sp7^{fl/fl;Col1a1-Cre}$) affected the trabecular bone volume differentially in males and females and in long bones and vertebrae, probably through differential levels in the accumulation of immature osteoblasts. In contrast, the femoral cortical bone was thin and porous in $Sp7^{floxneo/floxneo}$ and $Sp7^{fl/fl;Col1a1-Cre}$ mice of both sexes compared with the respective controls, which was caused by the increased bone resorption due to osteocyte apoptosis through the reduction in the number of osteocyte processes and canaliculi. These findings demonstrated that Sp7 inhibits the proliferation of immature osteoblasts and induces their differentiation, and that Sp7 regulates the process formation of osteoblasts, which is finally essential for the survival of embedded osteocytes and the development and maintenance of cortical bone.

Female $Sp7^{floxneo/floxneo}$ and $Sp7^{fl/fl;Col1a1-Cre}$ mice showed similar phenotypes and the femoral trabecular bone volume was increased, while femoral trabecular bone volume in male $Sp7^{floxneo/floxneo}$, $Sp7^{floxneo/floxneo;Col1a1-Cre}$, and $Sp7^{fl/fl;Col1a1-Cre}$ mice was similar to the respective controls. Although we could not perform all experiments in both sexes, BrdU-positive osteoblastic cells were increased in the trabecular bone of male $Sp7^{fl/fl;Col1a1-Cre}$ mice, and osteoblast parameters and bone formation rate increased in the trabecular bone of female $Sp7^{fl/fl;Col1a1-Cre}$ mice. These findings suggest that immature osteoblasts accumulated in the trabecular bone in both male and female $Sp7^{fl/fl;Col1a1-Cre}$ mice, but at different levels, compensating for the inhibited osteoblast maturation, as shown by the increased expression of the immature osteoblast marker gene *Spp1* and the reduced expression of the mature osteoblast marker gene *Bglap/Bglap2*. The increase in an early osteoblast differention marker, ALP, and the reduction of a late marker, mineralization, in the culture of primary osteoblasts from $Sp7^{fl/fl;Col1a1-Cre}$ mice were also compatible with the phenotypes. Thus, Sp7 was considered to inhibit the proliferation of osteoblast lineage cells and induces their differentiation. Estrogen and progesterone may be positively involved in the accumulation of immature osteoblasts in female $Sp7^{fl/fl;Col1a1-Cre}$ mice because they were previously shown to induce osteoblast proliferation and differentiation [23,24]. In contrast, the proliferation of osteoblastic cells was reduced in $Runx2^{fl/fl;Col1a1-Cre}$ mice, which were generated using the same 2.3-kb *Col1a1* promoter EGFP-Cre transgenic mice. Bone volume, osteoblast parameters, and bone formation in the femoral trabecular bone decreased in both males and females, clarifying the opposite functions of Sp7 and Runx2 in the proliferation of immature osteoblasts [19,25,26]. The decrease in the number of Sost-expressing osteocytes appeared to have contributed to the accumulation of immature osteoblasts in $Sp7^{fl/fl;Col1a1-Cre}$ mice by enhancing canonical Wnt signaling pathway [11].

Differential changes in femoral and vertebral trabecular bone volumes were observed in both male and female $Sp7^{fl/fl;Col1a1-Cre}$ mice. The differences in the femoral and vertebral trabecular bone were due to the number of osteoblasts and the bone formation rate (Fig. 4A–D). Recently, skeletal stem cells in vertebrae were shown to be different from those in limb bones, with a different gene expression profile [27]. Thus, the proliferation of osteoblast lineage cells and their differentiation in vertebrae and limb bones are likely to be regulated by different transcription factors and signaling pathways.

Bone formation in the femoral cortical bone of $Sp7^{fl/fl;Col1a1-Cre}$ mice was similar to that in $Sp7^{fl/fl}$ mice, but the number of osteoclasts in the cortical bone increased. Thus, the thin and porous cortical bone was attributed to enhanced bone resorption, likely owing to osteocyte apoptosis and necrosis. Among *SP7* mutations in humans, a homozygous mutation (R316C) and a heterozygous mutation in zinc finger 2 (E340A) cause osteogenesis imperfecta with high bone turnover and low bone turnover, respectively, and both patients have porous cortical bone [28,29]. Furthermover, the number and length of canaliculi are reduced in patients with the R316C mutation [9]. Although the lacunocanalicular structure was not examined in patients with the E340A mutation, the porous cortical bone in patients with the R316C or E340A mutation may have been caused by osteocyte death due to reductions in osteocyte processes and canaliculi.

The number of TRAP-positive cells increased in the cortical bone but not in the trabecular bone of $Sp7^{fl/fl;Col1a1-Cre}$ mice, probably because the frequency of TUNEL-positive lacunae in the cortical bone was much higher than that in the trabecular bone in $Sp7^{fl/fl;Col1a1-Cre}$ mice. This could be explained by two factors. Most osteocytes in the trabecular bone are close to the bone surface and easily obtain oxygen and nutrients for survival, even with a reduced number of processes. Furthermore, trabecular bone is remodeled faster than cortical bone, and apoptotic/necrotic osteocytes in trabecular bone are removed faster than those in cortical bone. The former reduces the number of apoptotic/necrotic osteocytes, while the latter reduces osteoclastogenesis induced by apoptotic/necrotic osteocytes. As osteoclastogenesis was enhanced in the co-culture of $Sp7^{fl/fl;Col1a1-Cre}$ primary osteoblasts and wild-type BMMs, however, the bone quality of $Sp7^{fl/fl;Col1a1-Cre}$ mice may have negatively affected osteoclastogenesis.

The frequency of Sost-positive osteocytes was lower in $Sp7^{fl/fl;Col1a1-Cre}$ mice than that in $Sp7^{fl/fl}$ mice (Fig. 6R). Direct regulation of the *Sost* gene by Sp7 was previously reported [4]. However, the frequency of Sost-positive osteocytes in the femur and the serum level of Sost in *Col1a1-Sp7* transgenic mice, which have fewer osteocyte processes and canaliculi, were also lower than those in wild-type mice [12]. Therefore, the impaired lacunocanalicular system in $Sp7^{fl/fl;Col1a1-Cre}$ mice and *Col1a1-Sp7* transgenic mice may also be responsible for the reduction in the frequency of Sost-positive osteocytes because the lacunocanalicular system is responsible for mechano-sensing and mechano-transduction, and Sost expression changes by mechanical loading [11,12,30–32].

Previous studies demonstrated that $Sp7^{fl/-;CAG-CreER}$ mice treated with tamoxifen and *Sp7* deletion by *Dmp1* Cre ($Sp7^{OcyKO}$) reduced the number of osteocyte processes and canaliculi [4,9]. Canalicular number was also reduced in $Sp7^{fl/fl;Col1a1-Cre}$ mice (Fig. 6Q). However, the number of osteocyte processes and canaliculi was also decreased in *Col1a1-Sp7* transgenic mice, and these reductions were larger than those in $Sp7^{fl/fl;Col1a1-Cre}$ mice (Fig. 6A–H, Q) [12,33]. As it is difficult for

osteocytes to form canaliculi after mineralization, the number of canaliculi will be determined by the number of cell processes at the transitional stage from osteoblasts to osteocytes. Based on these findings, therefore, an appropriate Sp7 level appears to be required for the final stage of osteoblasts to acquire a sufficient number of processes. It has been shown that the knockdown of *Sp7* reduces the number of processes in MC3T3-E1 cells, infection with an *Ostn*-expressing lentivirus restores this decrease, and AAV8-*Ostn* infection in $Sp7^{OcyKO}$ mice increases the number of canaliculi [9]. However, the expression of *Ostn* was not reduced in $Sp7^{OcyKO}$ femurs [9]; it was increased in the osteoblast-enriched fraction of $Sp7^{fl/fl;Col1a1-Cre}$ mice, and its expression in the osteocyte fraction of $Sp7^{fl/fl;Col1a1-Cre}$ mice and in the osteoblast and osteocyte fractions of *Col1a1-Sp7* transgenic mice were similar to those in the respective controls. Moreover, *Sp7* overexpression in MC3T3-E1 cells failed to induce *Ostn* (Fig. 7B–D). Therefore, the mechanisms underlying the regulation of osteoblast and osteocyte process formation warrant further investigation.

In conclusion, Sp7 is involved in osteoblast proliferation, osteoblast maturation, *Col1a1* expression, and process formation in committed osteoblasts. The compensatory mechanisms for impaired osteoblast maturation differed between femurs and vertebrae and between males and females and need to be clarified in the future. To maintain bone volume and quality, it is important to elucidate the mechanisms by which mature osteoblasts/osteocytes acquire a sufficient number of processes for osteocyte survival as well as mechano-sensing and mechano-transduction.

4. Materials and methods

4.1. Mice

Generation of $Sp7^{floxneo/floxneo}$ mice, 2.3-kb *Col1a1* EGFP-Cre transgenic mice, CAG-Flp transgenic mice, and osteoblast specific *Sp7* transgenic mice under the control of 2.3-kb *Col1a1* promoter has been previously described [6,19,33,34]. $Sp7^{floxneo/floxneo}$ mice contain a neomycin resistance gene (neo) in the *Sp7* intron. $Sp7^{floxneo/floxneo}$ mice were crossed with 2.3-kb *Col1a1* EGFP-Cre transgenic mice to generate $Sp7^{floxneo/floxneo;Col1a1-Cre}$ mice. $Sp7^{floxneo/floxneo}$ mice were crossed with CAG-Flp transgenic mice to remove neo, and $Sp7^{fl/fl}$ mice were generated. $Sp7^{fl/fl}$ mice were crossed with 2.3-kb *Col1a1* EGFP-Cre transgenic mice to generate $Sp7^{fl/fl;Col1a1-Cre}$ mice. The backgrounds of $Sp7^{floxneo/floxneo}$, $Sp7^{fl/fl}$, and CAG-Flp transgenic mice were C57BL/6. 2.3-kb *Col1a1* EGFP-Cre transgenic mice were generated in the B6C3H F1 background and backcrossed with C57BL/6 mice more than 14 times. Prior to the initiation of the study, all experimental protocols were reviewed and approved by the Animal Care and Use Committee of Nagasaki University Graduate School of Biomedical Sciences (No. 1903131520–9). Animals were housed three per cage in a pathogen-free environment on a 12-h light cycle at 22 °C ± 2 °C, with standard chow (CLEA Japan, Tokyo, Japan) and free access to tap water. All relevant guidelines for working with animals were adhered to in this study.

4.2. Real-time RT-PCR and western blot analysis

The osteoblast fraction was collected using a micro-intertooth brush (Kobayashi Pharmaceutical Co., Ltd., Osaka, Japan) from the endosteum of tibiae after bone marrow was flushed out by PBS, and the remaining bone was used for the osteocyte fraction, as previously reported [10]. Total RNA was extracted using ISOGEN (Wako, Osaka, Japan). Real-time RT-PCR was performed using THUNDERBIRD SYBR quantitative PCR (qPCR) Mix (Toyobo, Osaka, Japan) and Light Cycler 480 Real-Time PCR system (Roche Diagnostics, Tokyo, Japan). Primer sequences are shown in Supplemental Table 1. The primer set for *Bglap/Bglap2* detected both *Bglap* and *Bglap2*. The values obtained were normalized to those of actin beta (*Actb*) using the $2^{(-\text{delta delta C(t)})}$ method. Western blotting was performed using rabbit polyclonal anti-Sp7 (Abcam, Cambridge, UK) and anti-β-actin (Santa Cruz Biotechnology, Dallas, TX, USA) antibodies.

4.3. Micro-CT analysis

Micro-CT analysis was performed using a μCT system (R_mCT; Rigaku Corporation, Tokyo, Japan), except for the analysis of the first lumbar vertebra in male mice. Data from scanned slices were used in a three-dimensional analysis to calculate femoral morphometric parameters. Trabecular bone parameters were measured on the distal femoral metaphysis. Approximately 2 mm (0.2 mm from the growth plate) was cranio-caudally scanned and 200 slices at 10-μm increments were taken. In femoral cortical bone, 20 slices in 10-μm increments were taken. To analyze the first lumbar vertebra in female mice, 100 slices were obtained. The threshold of mineral density was 500 mg/cm^3. The first lumbar vertebra in male mice were scanned using a micro-CT system (Skyscan1176, Bruker, Aartselaar, Belgium), and 150 slices in 9-μm increments were obtained. The pore area in femoral cortical bone at the mid-diaphysis was measured by Skyscan 1272 (Bruker) at a resolution of 10 μm/voxel.

4.4. Bone histomorphometric analysis

Mice were intraperitoneally injected with calcein 7 and 2 days before sacrifice at a dose of 20 mg/kg body weight, and were examined at 10 weeks of age. Mice were euthanized and their tibiae, femurs, and lumbar vertebrae (L3–L5) were harvested and fixed in 70 % ethanol for three days. The fixed bones were dehydrated with graded ethanol, infiltrated and embedded in a mixture of methyl methacrylate and 2-hydroxyethyl methacrylate (Fujifilm Wako Pure Chemical, Osaka, Japan). Bone histomorphometric analysis of the proximal tibiae and lumbar vertebrae was performed using undecalcified 4-μm-thick sections, as previously described [35]. Bone histomorphometric analysis of cortical bone was conducted using approximately 50-μm-thick cross-sections from the mid-diaphyses of femurs. Structural, dynamic, and cellular parameters were calculated and expressed according to the standard nomenclature [36].

4.5. Serum testing

Blood was collected from the heart and left to stand at room temperature for at least 30 min. Serum was collected after centrifugation at 3000 rpm/min at room temperature for 10 min. Serum levels of P1NP and TRAP5b were measured using a Rat/Mouse P1NP enzyme-linked immunosorbent assay (Immunodiagnostic Systems, Boldon Business Park, UK) and Mouse TRAP Assay (Immunodiagnostic Systems), respectively.

4.6. Histological analysis

Mice were anesthetized and perfusion fixed in 4 % paraformaldehyde/0.1 M phosphate buffer (PFA), and femurs were separated and subjected to further oscillatory fixation with 4 % PFA at 4 °C overnight. After decalcification in 10 % EDTA, the bone samples were embedded in paraffin. Four-micrometer-thick sections were stained with hematoxylin and eosin (H-E), safranin O (Solarbio, Beijing, China), or fast red violet LB salt for TRAP (Absin, Shanghai, China). TUNEL staining was performed using an ApopTag Peroxidase In Situ Apoptosis Detection Kit (Sigma Aldrich, St. Louis, MO, USA) and counterstained with methyl green. To analyze BrdU incorporation, we injected BrdU intraperitoneally into 3-week-old mice at 100 μg/g body weight 1 h before sacrifice, and BrdU incorporation was detected using a BrdU staining kit (Invitrogen, Carlsbad, CA, USA). The sections were counterstained with hematoxylin. Bone canalicular staining (silver impregnation staining) was performed using Silver Protein (198–18101: FUJIFILM-Wako) according to a previously reported method [37].

BrdU-positive osteoblastic cells, TUNEL-positive lacunae, Sost-positive osteocytes, canalicular number, and Safranin O-positive area in trabecular bone were counted or measured in three enlarged trabecular areas and then averaged. TUNEL-positive lacunae, Sost-positive osteocytes, and the canalicular number in cortical bone were counted in four areas: anterior metaphyseal, posterior metaphyseal, anterior diaphyseal, and posterior diaphyseal cortical bones. TUNEL-positive osteoblasts were counted in three areas of the endosteum at the metaphysis. In the analysis of the canalicular number, at least 10 lacunae with live osteocytes were randomly selected, the number of canaliculi in each osteocyte was counted, and counts were averaged. In each experiment, one section was analyzed for each mouse. Immunohistochemistry was performed using polyclonal goat anti-Sost (R&D, Minneapolis, MN, USA), polyclonal rabbit anti-Sp7 (Abcam, Cambridge, UK), monoclonal rabbit anti-Runx2 (Cell Signaling, Danvers, MA, USA), and polyclonal rabbit anti-Col1a1 (Rockland, Limerick, PA, USA) antibodies. Secondary antibodies were Histofine Stain MAXPO (R) (Nichirei, Tokyo, Japan) for anti-Sp7, anti-Runx2, and anti-Col1a1 antibodies, and a goat two-step test kit (ZSGB-BIO, Beijing, China) for the anti-Sost antibody. Immunohistochemistry without the first antibodies resulted in no significant signals. To obtain frozen sections, newborn mice were euthanized and fixed in PFA at 4 °C for 2 h, washed with PBS at 4 °C for 1 h, immersed in 20 % sucrose at 4 °C overnight, embedded in optimum cutting temperature (O.C.T.) compound (Sakura Finetek, Tokyo, Japan), and sectioned at a thickness of 7 μm using a Leica CM3050S research cryostat (Leica Biosystems, Wetzlar, Germany).

4.7. Cell culture and Sp7 overexpression

Primary osteoblasts and osteoblast progenitors were isolated from the wild-type calvariae of newborn mice. The calvariae were cut into small pieces and cultured for 10–14 days in a three-dimensional collagen gel (Cell matrix, Nitta Gelatin, Co., Osaka, Japan) with α-modified Minimum Essential Medium (α-MEM) containing 10 % fetal bovine serum (FBS). Cells outgrowing from explants were retrieved by an incubation at 37 °C for 30 min with 0.2 % collagenase (Wako Pure Chemical Industries, Osaka, Japan) in PBS (−). In this method, the main cell types isolated were osteoblast progenitors and osteoblasts at an early differentiation stage with low ALP activity and virtually no *Bglap/Bglap2* production [38]. Cells were plated in 24-well plates at a density of 1.9×10^4 cells/cm^2 in αMEM supplemented with 10 % FBS. Cells were transfected with EGFP-expressing (pME18-EGFP) or type I *Sp7*-expressing (pME18-*Sp7*) vector using X-tremeGENE9 (Roche Diagnostics). Transfected cells were cultured for 48 h before RNA extraction.

4.8. In vitro osteoblastogenesis

Primary osteoblasts were isolated from the calvariae of $Sp7^{fl/fl}$ and $Sp7^{fl/fl;Col1a1-Cre}$ newborns by sequential digestion with 0.1 % collagenase A and 0.2 % dispase. Osteoblastic cells from the third to fifth fractions were pooled and used for osteoblast differentiation. Cells were seeded on 48-well plates at a density of 1.3×10^5 cells/cm^2, and medium was changed to osteogenic medium containing 50 μg/ml of ascorbic acid and 10 mM β-glycerophosphate at confluence. Staining for ALP and mineralization (von Kossa) was performed 5 and 13 days after confluence, respectively, as previously described [19].

4.9. In vitro osteoclastogenesis

BMMs were isolated by density gradient centrifugation using Ficoll–Paque™ (GE Healthcare, Tokyo, Japan) from the bone marrow of 10-week-old wild-type mice. BMMs at 2.5×10^5 cells/cm^2 were co-cultured with primary osteoblasts, which were prepared from the calvariae of $Sp7^{fl/fl}$ and $Sp7^{fl/fl;Col1a1-Cre}$ newborn mice using a three-dimensional collagen gel, at 1.3×10^4 cells/cm^2 in α-MEM containing 10 % FBS in the presence of 50 μg/ml of ascorbic acid and 10^{-8} M 1α,25 $(OH)_2D_3$ in 24-well plates for 8 days. TRAP staining was performed as previously described [39]. To assess bone resorption, BMMs at 5×10^4 cells/cm^2 were co-cultured with primary osteoblasts at 2.6×10^4 cells/cm^2 in α-MEM containing 10 % FBS in the presence of 50 μg/ml of ascorbic acid and 10^{-8} M 1α,25 $(OH)_2D_3$ on dentin slices (Wako) in 96-well plates for 13 days, and the resorbed area was measured by scanning electron microscopy (H-7100; Hitachi, Tokyo, Japan).

4.10. Graphical abstract

Gaphical abstract was drawed by Figdraw.

4.11. Statistical analysis

Values are shown as the mean ± SD. Statistical analyses were performed using the Student's *t*-test, and those of more than three groups were conducted by ANOVA and the Tukey–Kramer post-hoc test.

5. Category 3

Approval of the version of the manuscript to be published (the names of all authors must be listed):

Qing Jiang, Kenichi Nagano, Takeshi Moriishi, Hisato Komori, Chiharu Sakane, Yuki Matsuo, Zhiguo Zhang, Riko Nishimura, Kosei Ito, Xin Qin, Toshihisa Komori.

6. Article Processing Charge

The corresponding author agrees to pay the Journal of Orthopaedic Translation Article Processing Charge upon acceptance of the work for publication in Journal of Orthopaedic Translation, unless prior arrangements have been made to waive the Article Processing Charge.

Author names and details of the conflict(s) of interest

This *Authorship & Conflicts of Interest Statement* is signed by all the authors listed in the manuscript to indicate agreement that the above information is true and correct (*a photocopy of this form may be used if there are more than 10 authors*).

Disclosures

The authors declare that they have no conflicts of interest.

CRediT authorship contribution statement

Qing Jiang: Data curation, Formal analysis, Investigation, Methodology, Software, Validation, Funding acquisition. **Kenichi Nagano:** Investigation, Formal analysis, Methodology, Software, Funding acquisition. **Takeshi Moriishi:** Investigation, Methodology, Funding acquisition. **Hisato Komori:** Investigation, Funding acquisition. **Chiharu Sakane:** Investigation, Funding acquisition. **Yuki Matsuo:** Project administration, Investigation, Funding acquisition. **Zhiguo Zhang:** Methodology. **Riko Nishimura:** Methodology. **Kosei Ito:** Methodology. **Xin Qin:** Investigation, Data curation, Validation, Supervision, Writing – original draft, Funding acquisition. **Toshihisa Komori:** Data curation, Validation, Supervision, Writing – original draft, Writing – review & editing, Funding acquisition.

Declaration of competing interest

A conflict of interest occurs when an individual's objectivity is potentially compromised by a desire for financial gain, prominence, professional advancement or a successful outcome. The Editors of the *Journal of Orthopaedic Translation* strive to ensure that what is published

in the Journal is as balanced, objective and evidence-based as possible. Since it can be difficult to distinguish between an actual conflict of interest and a perceived conflict of interest, the Journal requires authors to disclose all and any potential conflicts of interest.

The authors whose names are listed immediately below certify that they have NO affiliations with or involvement in any organization or entity with any financial interest (such as honoraria; educational grants; participation in speakers' bureaus; membership, employment, consultancies, stock ownership, or other equity interest; and expert testimony or patent-licensing arrangements), or non-financial interest (such as personal or professional relationships, affiliations, knowledge or beliefs) in the subject matter or materials discussed in this manuscript.

Acknowledgments

This work was supported by grants from the Japanese Ministry of Education, Culture, Sports, Science and Technology, Japan to Toshihisa Komori (23H00440), Kenichi Nagano (19K10056), Takeshi Moriishi (23K09120), Hisato Komori (23K08591), Chiharu Sakane (22K11805), and Yuki Matsuo (24K12356), Key Laboratory of Orthopaedics of Suzhou (SZS2022017) to Qing Jiang and Xin Qin, and Priority Academic Program Development of Jiangsu Higher Education Institutions (PAPD), China to Qing Jiang and Xin Qin. We thank B. De Crombrugghe for the 2.3-kb *Col1a1* promoter, H. Kaneko for technical and secretarial assistances.

Appendix A. Supplementary data

Supplementary data to this article can be found online at https://doi.org/10.1016/j.jot.2024.06.005.

References

[1] Komori T. Whole aspect of Runx2 functions in skeletal development. Int J Mol Sci 2022;23:5776.
[2] Hojo H, Ohba S, He X, Lai LP, McMahon AP. Sp7/Osterix is restricted to bone-forming vertebrates where it acts as a Dlx co-factor in osteoblast specification. Dev Cell 2016;37:238–53.
[3] Nakashima K, Zhou X, Kunkel G, Zhang Z, Deng JM, Behringer RR, et al. The novel zinc finger-containing transcription factor Osterix is required for osteoblast differentiation and bone formation. Cell 2002;108:17–29.
[4] Zhou X, Zhang Z, Feng JQ, Dusevich VM, Sinha K, Zhang H, et al. Multiple functions of Osterix are required for bone growth and homeostasis in postnatal mice. Proc Natl Acad Sci USA 2010;107:12919–24.
[5] Wang JS, Tokavanich N, Wein MN. SP7: from bone development to skeletal disease. Curr Osteoporos Rep 2023;21:241–52.
[6] Nishimura R, Wakabayashi M, Hata K, Matsubara T, Honma S, Wakisaka S, et al. Osterix regulates calcification and degradation of chondrogenic matrices through matrix metalloproteinase 13 (MMP13) expression in association with transcription factor Runx2 during endochondral ossification. J Biol Chem 2012;287:33179–90.
[7] Baek WY, Lee MA, Jung JW, Kim SY, Akiyama H, de Crombrugghe B, et al. Positive regulation of adult bone formation by osteoblast-specific transcription factor Osterix. J Bone Miner Res 2009;24:1055–65.
[8] Baek WY, Crombrugghe B, Kim JE. Postnatally induced inactivation of Osterix in osteoblasts results in the reduction of bone formation and maintenance. Bone 2010;46:920–8.
[9] Wang JS, Kamath T, Mazur CM, Mirzamohammadi F, Rotter D, Hojo H, et al. Control of osteocyte dendrite formation by Sp7 and its target gene osteocrin. Nat Commun 2021;12:6271.
[10] Moriishi T, Maruyama Z, Fukuyama R, Ito M, Miyazaki T, Kitaura H, et al. Overexpression of Bcl2 in osteoblasts inhibits osteoblast differentiation and induces osteocyte apoptosis. PLoS One 2011;6:e27487.
[11] Moriishi T, Fukuyama R, Ito M, Miyazaki T, Maeno T, Kawai Y, et al. Osteocyte network; a negative regulatory system for bone mass augmented by the induction of Rankl in osteoblasts and Sost in osteocytes at unloading. PLoS One 2012;7:e40143.
[12] Moriishi T, Ito T, Fukuyama R, Qin X, Komori H, Kaneko H, et al. Sp7 transgenic mice with a markedly impaired lacunocanalicular network induced Sost and reduced bone mass by unloading. Int J Mol Sci 2022;23:3173.
[13] Kennedy OD, Laudier DM, Majeska RJ, Sun HB, Schaffler MB. Osteocyte apoptosis is required for production of osteoclastogenic signals following bone fatigue in vivo. Bone 2014;64:132–7.
[14] Buckley KA, Hipskind RA, Gartland A, Bowler WB, Gallagher JA. Adenosine triphosphate stimulates human osteoclast activity via upregulation of osteoblast-expressed receptor activator of nuclear factor-kappa B ligand. Bone 2002;31:582–90.
[15] Cheung WY, Fritton JC, Morgan SA, Seref-Ferlengez Z, Basta-Pljakic J, Thi MM, et al. Pannexin-1 and P2X7-receptor are required for apoptotic osteocytes in fatigued bone to trigger RANKL production in neighboring bystander osteocytes. J Bone Miner Res 2016;31:890–9.
[16] Komori T. Cell death in chondrocytes, osteoblasts, and osteocytes. Int J Mol Sci 2016;17:2045.
[17] Zong WX, Thompson CB. Necrotic death as a cell fate. Genes Dev 2006;20:1–15.
[18] Lotze MT, Tracey KJ. High-mobility group box 1 protein (HMGB1): nuclear weapon in the immune arsenal. Nat Rev Immunol 2005;5:331–42.
[19] Qin X, Jiang Q, Komori H, Sakane C, Fukuyama R, Matsuo Y, et al. Runt-related transcription factor-2 (Runx2) is required for bone matrix protein gene expression in committed osteoblasts in mice. J Bone Miner Res 2021;36:2081–95.
[20] Nishio Y, Dong Y, Paris M, O'Keefe RJ, Schwarz EM, Drissi H. Runx2-mediated regulation of the zinc finger Osterix/Sp7 gene. Gene 2006;372:62–70.
[21] Li X, Zhang Y, Kang H, Liu W, Liu P, Zhang J, et al. Sclerostin binds to LRP5/6 and antagonizes canonical Wnt signaling. J Biol Chem 2005;280:19883–7.
[22] Semenov M, Tamai K, He X. SOST is a ligand for LRP5/LRP6 and a Wnt signaling inhibitor. J Biol Chem 2005;280:26770–5.
[23] Ernst M, Heath JK, Schmid C, Froesch RE, Rodan GA. Evidence for a direct effect of estrogen on bone cells in vitro. J Steroid Biochem 1989;34:279–84.
[24] Scheven BA, Damen CA, Hamilton NJ, Verhaar HJ, Duursma SA. Stimulatory effects of estrogen and progesterone on proliferation and differentiation of normal human osteoblast-like cells in vitro. Biochem Biophys Res Commun 1992;186:54–60.
[25] Kawane T, Qin X, Jiang Q, Miyazaki T, Komori H, Yoshida CA, et al. Runx2 is required for the proliferation of osteoblast progenitors and induces proliferation by regulating Fgfr2 and Fgfr3. Sci Rep 2018;8:13551.
[26] Qin X, Jiang Q, Miyazaki T, Komori T. Runx2 regulates cranial suture closure by inducing hedgehog, Fgf, Wnt and Pthlh signaling pathway gene expressions in suture mesenchymal cells. Hum Mol Genet 2019;28:896–911.
[27] Sun J, Hu L, Bok S, Yallowitz AR, Cung M, McCormick J, et al. A vertebral skeletal stem cell lineage driving metastasis. Nature 2023;621:602–9.
[28] Fiscaletti M, Biggin A, Bennetts B, Wong K, Briody J, Pacey V, et al. Novel variant in Sp7/Osx associated with recessive osteogenesis imperfecta with bone fragility and hearing impairment. Bone 2018;110:66–75.
[29] Ludwig K, Ward LM, Khan N, Robinson ME, Miranda V, Bardai G, et al. Dominant osteogenesis imperfecta with low bone turnover caused by a heterozygous SP7 variant. Bone 2022;160:116400.
[30] Robling AG, Niziolek PJ, Baldridge LA, Condon KW, Allen MR, Alam I, et al. Mechanical stimulation of bone in vivo reduces osteocyte expression of Sost/sclerostin. J Biol Chem 2008;283:5866–75.
[31] Lin C, Jiang X, Dai Z, Guo X, Weng T, Wang J, et al. Sclerostin mediates bone response to mechanical unloading through antagonizing Wnt/beta-catenin signaling. J Bone Miner Res 2009;24:1651–61.
[32] Moustafa A, Sugiyama T, Prasad J, Zaman G, Gross TS, Lanyon LE, et al. Mechanical loading-related changes in osteocyte sclerostin expression in mice are more closely associated with the subsequent osteogenic response than the peak strains engendered. Osteoporos Int 2012;23:1225–34.
[33] Yoshida CA, Komori H, Maruyama Z, Miyazaki T, Kawasaki K, Furuichi T, et al. SP7 inhibits osteoblast differentiation at a late stage in mice. PLoS One 2012;7:e32364.
[34] Otani S, Date Y, Ueno T, Ito T, Kajikawa S, Omori K, et al. Runx3 is required for oncogenic Myc upregulation in p53-deficient osteosarcoma. Oncogene 2022;41:683–91.
[35] Qin X, Jiang Q, Nagano K, Moriishi T, Miyazaki T, Komori H, et al. Runx2 is essential for the transdifferentiation of chondrocytes into osteoblasts. PLoS Genet 2020;16:e1009169.
[36] Dempster DW, Compston JE, Drezner MK, Glorieux FH, Kanis JA, Malluche H, et al. Standardized nomenclature, symbols, and units for bone histomorphometry: a 2012 update of the report of the ASBMR Histomorphometry Nomenclature Committee. J Bone Miner Res 2013;28:2–17.
[37] Kusuzaki K, Kageyama N, Shinjo H, Takeshita H, Murata H, Hashiguchi S, et al. Development of bone canaliculi during bone repair. Bone 2000;27:655–9.
[38] Komori T, Yagi H, Nomura S, Yamaguchi A, Sasaki K, Deguchi K, et al. Targeted disruption of Cbfa1 results in a complete lack of bone formation owing to maturational arrest of osteoblasts. Cell 1997;89:755–64.
[39] Maruyama Z, Yoshida CA, Furuichi T, Amizuka N, Ito M, Fukuyama R, et al. Runx2 determines bone maturity and turnover rate in postnatal bone development and is involved in bone loss in estrogen deficiency. Dev Dynam 2007;236:1876–90.